CHALMERS
UNIVERSITY OF TECHNOLOGY

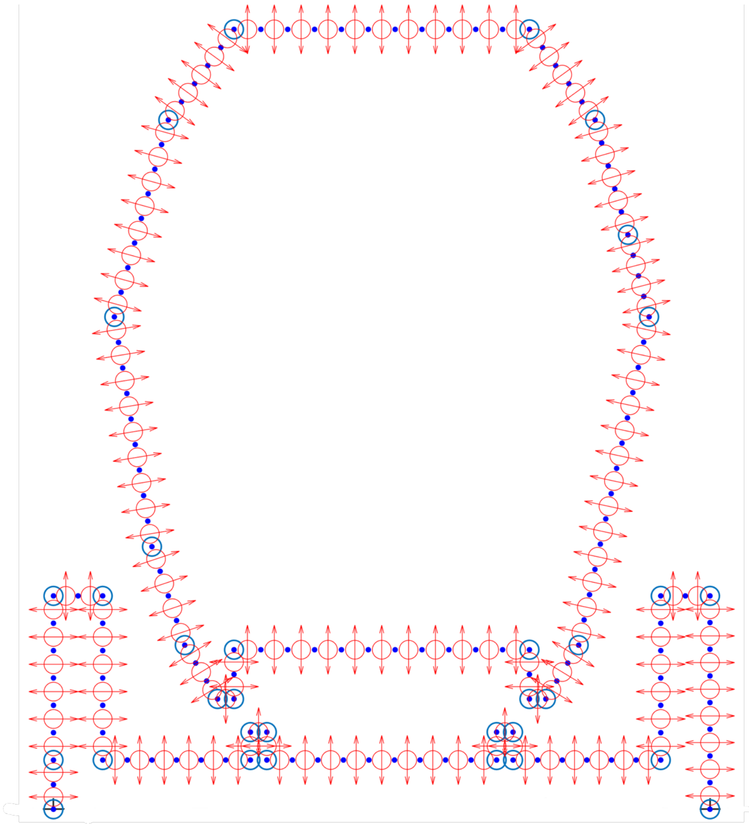

Investigation of Prediction Methods for Low Height Noise Barrier Implementation

Master's Thesis in Applied Acoustics

PATRIK ERIKSSON

DEPARTMENT OF ARCHITECTURE AND CIVIL ENGINEERING

CHALMERS UNIVERSITY OF TECHNOLOGY
Gothenburg, Sweden 2022
www.chalmers.se

Master's thesis 2022

An Investigation Of Prediciton Methods for Low Height Noise Barrier Implementation

PATRIK ERIKSSON

Department of Architechture and Civil Engineering
Division of Applied Acoustics
Chalmers University of Technology
Gothenburg, Sweden 2022

An investigation of prediction methods for low height noise barrier implementation
PATRIK ERIKSSON

Supervisor: Magnus Källman, Trafikverket/Swedish Transport Administration
Examiner: Jens Forssén, Division of Applied Acoustics

Master's Thesis 2022
Department of Architecture and Civil Engineering
Division of Applied Acoustics
Chalmers University of Technology
SE-412 96 Gothenburg
Telephone +46 31 772 1000

Cover: Image of an X60 - Commuter train model generated using the BEM numerical simulation model.

Typeset in LaTeX
Printed by Chalmers Reproservice
Gothenburg, Sweden 2022

An investigation of prediction methods for low height noise barrier implementation
PATRIK ERIKSSON
Department of Architecture and Civil Engineering
Chalmers University of Technology

Abstract

In areas where the more common tall noise screens produce an unreasonably large reduction on the quality of the urban environment, absorbing low height noise screens, in short LHNSs, can be introduced. Due to the screens relatively low height and the fact that they benefit from a placement as close to the source as possible, the visual impact on the environment is small. Furthermore studies have shown them to be cost effective and produce equal, or in some cases, higher attenuation than their more traditional counterparts.

However, due to the scale and cost of projects regarding railway infrastructure there is small room for error. Because of this, the current uncertainties in the prediction methods are often enough to warrant the usage of other noise reducing devices even though the LHNS could be viable solution.

To give the Swedish Transport Administration a solid basis on which to perform calculated estimates an investigation is launched. A literature study shows that to make good estimations of the sound field from a train screened with a LHNS, a combination of more traditional methods and numerical simulations are required. It also shows the importance of an accurate source model including the relative energy distribution between the sub-sources of a train.

Based on the findings a model utilising the 2.5D boundary element method is implemented to simulate the pressure field with and without screen for different train shapes. Geometrical estimations of a X60 commuter train, an empty industrial wagon and a case without a wagon are studied. The low height noise screen was modelled after the dimensions of an S-block 250.

The simulations show that a reasonably good fit to measurement data from other projects can be achieved in third-octave bands. However, in some cases, large deviations can be noted. Because of this further validations with a designated test setup is advised before drawing any definitive conclusions. Apart from the identified large deviations the results calculated here consistently show that a considerable reduction can be achieved by the implementation of LHNSs and that they warrant further consideration in future infrastructure projects.

Keywords: low-height noise screen, train, railway, STA, BEM, 2.5D-Geometry, Nord2000, insertion loss, NRD.

Acknowledgements

First and foremost I would like to thank Magnus Källman, Monica Waaranperä and Jens Forssén for their invaluable support during our consultancy session. A big thank you to Niclas Erlandsson for providing useful input and measurement-data. Also, thank you Jannik Theyssen for your input on the source distrubution, it really put me in the right direction.

Patrik Eriksson, Gothenburg, June 2022

List of Acronyms

Below is the list of acronyms that have been used throughout this thesis listed in alphabetical order:

IL	Insertion Loss
LHNS	Low Height Noise Screen
NDR	Noise Reducing Device
KHI	Kirchhoff-Helmholtz Integral
BEM	Boundary Element Method
STA	Swedish Transport Administration

Nomenclature

Below is the nomenclature of indices, sets, parameters, and variables that have been used throughout this thesis.

Indices

i,j	In chapter 2, Possible source(i) and receiver(j) locations
i,j	In chapter 3, Possible source(i) and receiver(j) locations outside of $\mathcal{V}_{BST}$ on $\mathcal{S}_{surf}$ and inside $\mathcal{V}_{free}$
im	The m:th frequency caluculated

Sets

$\mathcal{S}_T$	Set of points on the surface of the train model
$\mathcal{S}_{BS}$	Set of points on the surface of the ballast and the LHNS model
$\mathcal{S}_{surf}$	Total set of points including both train, ballast and LHNS
$\mathcal{V}_T$	Set of points in the volume enclosed by $\mathcal{S}_T$
$\mathcal{V}_{BS}$	Set of points in the volume enclosed by $\mathcal{S}_{BS}$
$\mathcal{V}_{BST}$	Set of points containing both volumes $\mathcal{V}_T$ and $\mathcal{V}_{BS}$
$\mathcal{V}_{free}$	Set of points in the volume containing $\mathcal{V}_{BST}$

Parameters and Variables in Order of Appearance

L_{w_0}	Sound power per meter of rail
L_{w_t}	Maximum sound power of a passing train
a,b	Train specific tuning parameters in Nord 96
v	Speed of a passing train
$L_{p,n96}$	Sound pressure level at some receiver point by the Nord 96 model
$\Delta L_{prop,n96}$	Attenuation by the Nord 96 propagation model

$L_{p,ij}$	Sound pressure level from source i at receiver j
ΔL_{ij}	Combined attenuation from directivity and propagation between source i and receiver j
r_{ij}	Distance between source i and receiver j
$L_{w,ij}$	Source term for position i,j
$L_{ref,j}$	Sub source strength at position j
$\Delta L(\varphi_j)$	Horizontal directivity
$\Delta L(\psi_j)$	Vertical directivity
$L_{p,n2k}$	Sound pressure level at some receiver point by the Nord 2000 model
L_w	Sound power level of the Nord 2000 source model
$\Delta L_{prop,n2k}$	Attenuation of the Nord 2000 propagation model
q_0	Some source with arbitrary source strength
x_s	Some source position inside of $\mathcal{V}_{free}$ outside of $\mathcal{V}_{BST}$
x_r	Some receiver position inside of $\mathcal{V}_{free}$ outside of $\mathcal{V}_{BST}$
$p(x_r)$	pressure at receiver location x_r
k	Wavenumber
R	Distance between source location x_s and receiver location x_r
$\vec{e}_{R_j}$	Unit vector in the direction from the source to the receiver
$\vec{n}_{S_j}$	Unit vector normal to the surface $\mathcal{S}_{surf}$
N	The amount of discretised segments
p_{q_0}	Pressure from the source q_0 inside of $\mathcal{V}_{free}$
p_{tot}	Total pressure from all contributing sources
N_{ch}	The amount of chief points inside of $\mathcal{V}_T$ and $\mathcal{V}_{BS}$ respectively
d_{max}	Largest geometrical length in the model
C_{PPW}	Chief points per wavelength fitting in d_{max}
x	Case x
c_0	Speed of sound in air
f	Frequency
p_{2D}	Two dimensional pressure calculated using the Kirchhoff-Helmholtz integral
p_{3D}	Estimation of the 3D pressure by implementing 2.5D geometry on the 2D pressure
Θ	Angle of the direct path of the source relative the XZ-plane
R_{Ew}	Source energy distribution weighting for the rail sources
W_{Ew}	Source energy distribution weighting for the wheel sources

$p_{0,rail}$	Modelled pressure from the rail source
$p_{0,wheel}$	Modelled pressure from the wheel sources
p_{Ew}	Sum of the weighted rail and wheel sources
Lp_{Deq}	Average modelled pressure level over angle Θ
$IL_{Ew,Deq}$	Energy weighted, angle equivalent insertion loss
$IL_{Ew,0^\circ}$	Energy weighted, maximum insertion loss
$IL_{Aeq,Ew,Deq}$	A - weighted average of $IL_{Ew,Deq}$
$IL_{Aeq,Ew,0^\circ}$	A - weighted average of $IL_{Ew,0^\circ}$

Contents

List of Figures

List of Tables

1
Introduction

1.1 Background

Low height noise screens (**LHNS**) are a type of noise reducing device (**NRD**) most commonly placed alongside transportation infrastructure where tall noise screens cause an unacceptable restriction of e.g. the quality of the living environment. The screen is designed in such a way that it benefits from a placement as close as possible to the source. As they are low in height the ability for actual screening of the sound is limited. Instead they rely on dampening and special geometrical designs to achieve attenuation of the direct and reflected sound. One of the major drawbacks of this approach is that the insertion loss (**IL**) can no longer be correctly estimated by most of the traditionally used methods based on low order geometrical ray-acoustics. This is partly because of their inability to handle more complex diffraction and reflection patterns.

In [10] a thorough investigation of the functional and economical limitations show that LHNSs are an inexpensive and viable alternative to high screens. However, because of the inaccuracy of the estimations made using available methods the LHNS often fall short in the planning process and the more 'safe' alternative of standard tall screens are used despite the possible advantages.

In an effort to implement a wider usage of the LHNSs the Swedish Transport Administration (**STA**) wants to investigate what methods can be used to give a good estimation of the IL when implementing LHNSs alongside the railway infrastructure in Sweden.

This thesis can be viewed as a railway-specific extension on the work made by C. Burgos and L. Wåssén on LHNS implemented along side of roads [11]. It is a most recommended read as it provides a great deal of insight regarding the concept, structure and limitations of the LHNS. One of the main differences between the screens used in road-side and railway applications is how regulations dictates the possible placement and design. For example: to enable placement as close to the source as possible in road side applications the screen should not exceed 1.1 m because this would cover the line of sight of the driver [11]; on the other hand for railway applications this height is 0.73 m above the top of the rail to not restrict on free space standard [12].

1.2 Purpose

The purpose of this thesis is to investigate how to accurately estimate the IL of LHNSs. By doing so provide STA with a solid basis to use in planning process of railway infrastructure and enable a wider usage of the LHNS as a NRD.

1.3 Scope

Due to the previous work made in [11], work into describing the function, practical limitations, construction and other LHNS-specific parameters will not be done. Instead the primary focus of the thesis will be to investigate what relevant methods can be used to calculate the IL and what their respective limitations are. To do this only tested and proven methods will be examined and used. No attempt to modify or build upon existing methods or theory will be made. As the focus of the thesis will be on the IL rather than the actual sound power levels, some arbitrary source strength will be used. Instead, because of the relatively low height of these barriers and their sensitivity in relation to the height of the source, the available source models will require a closer examination.

All geometrical estimations regarding the train and railway design is made in accordance to Swedish regulations and standards. The LHNS used in this case is modelled after a S-block 250 [5]. The screen height is 0.73 m and fulfil the requirement in [13] and [12] to be placed at 1.7 m from the centre of the track.

In the scope of this thesis the focus is to investigate the rail close, low height noise screens. However the model is not limited for usage in this type of investigation only and can be used to investigate the sound field around a variety of different applications.

The thesis will investigate IL of implementing a single LHNS for three different cases, a X60 train, a industrial train and no train (just track and screen)

1.4 Structure

To satisfy the goals of the project this thesis will attempt to answer five main questions:

1. What calculation methods are available and relevant to the project?
2. What are the, if any, limitations of these methods?
3. Is the information provided from answering question 1 and 2 enough to make accurate estimations?
4. How can the methods be used to model the IL of a LHNS?
5. How can the model be further improved upon?

To answer these questions the thesis will be divided into three main chapters. In Chapter 2 the findings from the literature study is compiled and presented. Information deemed useful and provide good insight into the process will also be included. Every piece of information will not be utilised in the thesis, it is however included to provide STA with a solid basis for continuation of the work. In Chapter 3 an in-depth presentation of the modelling theory, implementation and tuning is made. Furthermore a presentation of how the post processing of the modelled data is made is included. In Chapter 4 the setup used in the model is presented. This includes geometrical designs, source and receiver positions. Furthermore the acquisition process of the validation data as well as the data itself is presented.

2

Review of LHNS Calculation Methods

To answer question 1,2 and 3 stated in section 1.4 a literature study was conducted. The focus of the study was to find relevant methods that could be used to estimate the IL of LHNSs. One of the main concerns that the STA have with the current methods is that lack sufficient scientific testing and validation. Furthermore the currently used methods does not provide for the ability to do investigations of more complex geometries. Therefore the study focused on finding methods and work that has been done based on well documented theory. Additionally, these methods should be detailed enough to be able to properly account for the effect of complex geometrical designs.

As the Nordic propagation models are well known and widely used to estimate sound generated from rail bound traffic, it was an intuitive place to start by reviewing how these models accounts for a LHNS. Early on in the study it became quite clear that because of the low height and special function of the LHNS, the classical approaches lacked integration of the necessary parameters. For example: One way of estimating the effect a noise screen have on sound propagation is by Pierces thin hard diffracting screen solution. However, because the LHNSs rarely are thin and rely on absorption in multiple reflections it will not be properly estimated. In the Nord 2000 model the recommended approach is to use numerical simulations such as BEM, more on this in section 2.2.1.2.

Upon finding this information the focus of the study shifted to reviewing how numerical simulation methods could be implemented and what available methods/software could be used. One notable thing this showed, apart from information on the numerical methods, was the importance of an accurate source model, which became a point of interest and a closer review on this subject was made.

In summary the study showed that Nord 96 and Nord 2000 both provide for a simple and a detailed way to estimate the attenuation caused by propagation, but they fail in the proper estimation of the IL of a LHNS. Instead , if accurate and integrable estimations of the IL could be made with numerical methods, these models would provide for a well documented and reliable way of calculating the sound pressure generated by a passing train. The results could also be integrated into the SOUNDPLAN-software or adapted for usage with the Tyréns method[14] to further extend its usability.

To provide for a better overview and give some insight into where the parameters that needs change are coming from a shallow review of the Nordic propagation models will be presented in this chapter. Furthermore the source models used and some of the complications regarding their usage will also be reviewed.

2.1 Basic Concept of an Absorbent LHNS

In general a LHNS, unlike the standard high screens, work by adding some form of absorbent material to the side of the barrier facing the sound source. Because the screen is placed relatively close to the source the extra attenuation from an increased propagation path will not be significant. Instead the screen relies on the absorption in the barrier, train and ballast to absorb energy in numerous reflections as seen in Figure 2.1. This is one of the reasons why most conventional calculation methods based in geometrical ray acoustics fail to properly estimate the IL of a LHNS. They either rely on diffraction and/or ray tracing of the direct sound and reflections up to about the third degree.

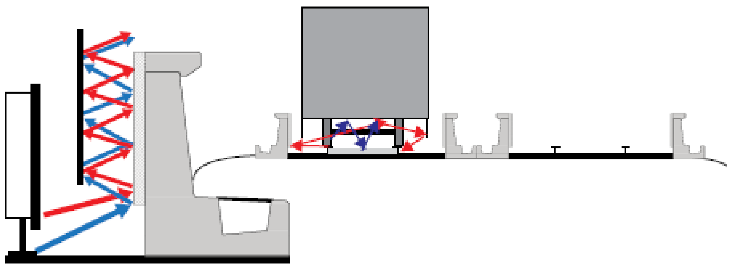

Figure 2.1: Illustrations of the concept of a S-block [1]. The sound waves generated by rail and wheel, blue and red respectively, is reflected against the screen several times by the undercarriage and boogie of the train.

2.2 Nordic Propagation Models

In this section a brief review of the Nordic propagation models will be presented. Even though the Nord 96 model is outdated it requires a mention due to the fact that Nord 2000 source model uses the Nord 96 data as a basis. It also provides for a good 'quick' estimation method by using the Tyréns method.

2.2.1 Nord 96 (NMT)

The official title of the report is *Railway Traffic Noise - Nordic Prediction Method* but is commonly refered to as Nord 96 or NMT. The model is a revision of the very basic old Nordic calculation method and includes, among other things, a way of estimating the generated sound effect per meter of trafficked rail by

$$L_{w_0} = a \log \frac{v}{100} + 10 \log l_{24} + b \text{ (dB re. } 10^{-12}\ W) \tag{2.1}$$

where a and b values are train model specific parameters, v is the speed of the passing train and l_{24} is the total length of train that has passed the receiver over a period of 24 hours. In a similar way the max value of the sound power can be estimated by

$$L_{w_t} = a \log \frac{v}{100} + 10 \log v + 43,8 + b \text{ (dB re. } 10^{-12}\ W) \tag{2.2}$$

These source models are then used in equation along side different corrections parameters in the propagation model

$$L_{p,n96} = \underbrace{L_{w_{0/t}}}_{\text{Source model}} + \underbrace{\Delta L_c + \Delta L_d + \Delta L_a + \Delta L_g + \Delta L_S + \Delta L_V + \Delta L_R}_{=\Delta L_{prop,n96}} \tag{2.3}$$

where $L_{w_{0/t}}$ is the generated sound effect calculated using 2.1 or 2.2 and the other $\Delta L_{c/d/a/g/S/V/R}$ terms are different attenuation parameters from the propagation model. It is here that the sought after information ΔL_S ,which is the screen effect, is found. Nord 96 assumes the screens to be hard and thin and uses geometrical acoustics to calculate the difference in propagation path between the case with and without screen. This will not properly account for the numerous reflections under the boogie, thus the model is unviable for usage in the estimation of a LHNS.

To solve this problem the Swedish consultancy firm Tyréns proposed in the report *Akustisk Prestanda S-Block* [14] to adjust the a & b parameters in equation 2.1 and 2.2 to fit with reference measurements of a case when LHNS have been implemented.

2.2.1.1 Nord 2000 - Rail Prediction Method

The most recent work on rail noise done within the frame of the comprehensive Nord 2000 model is the Rail prediction method [6].

This method has, among other things, included the ability to model tunnel openings as sources and increased the available spectrum of calculations to third octave bands ranging from 25 Hz to 10 kHz. A more detailed source model is also used.

According to the model the sound pressure at the receiver is

$$L_{p,ij} = L_{W,ij} + \Delta L_{ij} \text{ (dB re. 20 µPa)} \tag{2.4}$$

To account for directivity and propagation effects

$$\Delta L_{ij} = -10\log(4\pi r_{ij}^2) + \Delta L_{prop,n2k} \text{ (dB re. 20 µPa)} \tag{2.5}$$

where r is the distance between point ij and receiver and L_{prop} attenuation of the propagation model described in equation 2.4. The source term $L_{W,ij}$ is calculated by

$$L_{W,ij} = L_{Wref,j} + \Delta L\left(\varphi_j\right) + \Delta L\left(\psi_j\right) \text{ (dB re. 20 µPa)} \tag{2.6}$$

where $L_{Wref,j}$ is the sub-source strength for a specific train, $\Delta L\left(\varphi_j\right)$ and $\Delta L\left(\psi_j\right)$ is the horizontal and vertical correction factors respectively. More on this in section 2.4. The model provides for methods to estimate the amplifying effects of barriers such as tall buildings and in street canyons, but for actual screen effects it relies on the information provided in the comprehensive model [15].

2.2.1.2 Nord 2000 - Comprehensive Method

In the comprehensive model [15] the pressure level at a receiver for each frequency band is

$$L_{p,n2k} = \underbrace{L_W}_{\text{Source model}} + \underbrace{\Delta L_d + \Delta L_a + \Delta L_t + \Delta L_S + \Delta L_r}_{=\Delta L_{prop,n2k}} \text{ (dB re. 20 µPa)} \tag{2.7}$$

where L_W is the sound power level within the considered spectrum using the Nord 2000 source model. As in the case of Nord 96, it is here that the sought after information ΔL_S, the screen effect is found.

In the comprehensive Nord 2000 propagation model Hadden and Pierces diffracting wedge theory is utilised and modified to account for the absorbing effects in screens having one or two diffracting edges [15]. However the multiple reflections between the train and the LHNS will encounter far more than two diffracting edges and as a results a portion of the contributing sources will fail to be accounted for. Even though this method is better suited than Nord 96 this limitation makes it unviable for accurate estimations. To solve this problem Nord 2000 recommends using numerical calculation methods such as BEM to get estimations of the IL and using a correction factors based on the difference between a thin hard screen calculated using Pierce´s diffracting screen theory and numerical calculations [15].

In summary, to calculate the screen effect with the purpose of integrating the results in the Nord 2000 propagation model the following steps have to be done:

1. Calculate the effect of the screen using the methods provided in the model.
2. Estimate the IL of the screen by numerical simulations.
3. Estimate the IL of the same screen using Pierce´s thin hard screen solution.
4. Calculate the difference between case 2 and 3
5. Add the resulting difference to the original estimation as extra attenuation.

2.3 Numerical Calculation Methods

As a result of the review on the Nordic propagation models it is clear that to accurately estimate the screen effect of a LHNS, some form of numerical simulation is needed. A very well documented and tested numerical simulation method for radiation problems is the Boundary Element Method or in short **BEM**. P. Jean has made great success in adopting and using BEM to calculate the IL of a LHNS and similar NRDs [16][17]. In [18] an interesting and relevant point on the importance of using an incoherent line-source to accurately model noise barriers when doing BEM simulations is made. However when a line-source is used in 2D simulations it is assumed to be a homogeneous extension of a point source as so called, a coherent line-source. To make it incoherent a 3D-geometry have to be introduced. The source can now be modelled as an line of incoherent point-sources as so called, a incoherent line-source. The problem with this is that in most 3D-cases, simulations on a larger scale tend to be almost impossible due to the computational load. To solve this the concept of 2.5D-geometry developed by D. Duhamel [19] is introduced. This method enables the pressure field generated by an incoherent line-source to be implemented using fourier type integration on a pre-calculated 2D-BEM solution. This is the so called 2.5D-BEM simulation method. Based on this a software is made in [20] called MICADO.

In [21] A. Joliboi has made great success in accurately estimating the acoustic performance of LHNS using MICADO. The usage of the actual software have to be commissioned and it is therefore not within the scope to use in this thesis. However some of the concepts used in the report, mainly the 2.5D-geometry theory, is an excellent tool to provide better accuracy when estimating the IL of a LHNS.

On a side note, the acoustic module in COMSOL provides the ability to do both 2D- and 3D-BEM simulations. Some exploratory simulations where made but the size of the model made the calculation times very long. Furthermore due to lack of experience with the software, tuning and other software specific parameters made progress slow. In the end the software was deemed to complicated and unavailable for usage in this thesis.

Even though there are a variety of other methods that could be used to numerically simulate a LHNS, BEM became the intuitive way to go because of the authors previous knowledge in using the method. Furthermore a readily available MATLAB-script initially written by B. Van Der Aa for simulations on sonic crystals [22] and later revised by J. Forssén for use in [23] could be used. The script was further revised to enable the implementation of more complex geometries by the author. A more thorough review of BEM-theory and its implementations in the code will be presented in Chapter 3. Some notable numerical methods mentioned in [22] are presented here to provide for a future informational reference in similar projects. Therefore they are only named with no further information specified

- Finite Difference Time-Domain method (FDTD)
- Fast Field Program (FFP)
- Equivalent Sources Method
- Parabolic Equation Method (PE)
- Pseudo-Spectral Time-Domain Method (PSTD)

2.4 The Train As A Source

Due to the relatively low height and track-proximity, the shadow zone of a LHNS is sensitive to the vertical and horizontal placement of the source. A detailed source model is therefore important to make accurate IL estimations. Furthermore a good estimation of the train geometries and the surrounding objects are necessary to properly model the diffracted and scattered sound field. To achieve this the source models of the Nordic propagation models and research into the relative energy distribution between the sub-sources of a train are examined.

2.4.1 Train Source Models

From the bottom up the source model of a train typically contains contributions from [6]:

- Sleepers
- Rail
- Wheel
- Aero dynamic boogie noise
- Engine(relevant for diesel driven trains at low frequencies)
- Aerodynamic noise from the panthograph

One more noise source that could be relevant but is not included in the model is the AC and cooling fans mounted on the side of boogie. Both Nord 96 and Nord 2000 propose source models to be used in their respective propagation models. In Figure 2.2 the source model used in Nord 96 is presented. Here the source is assumed to be a point source located at the specified heights above the midpoint of the track. No information of the relative energy distribution is available.

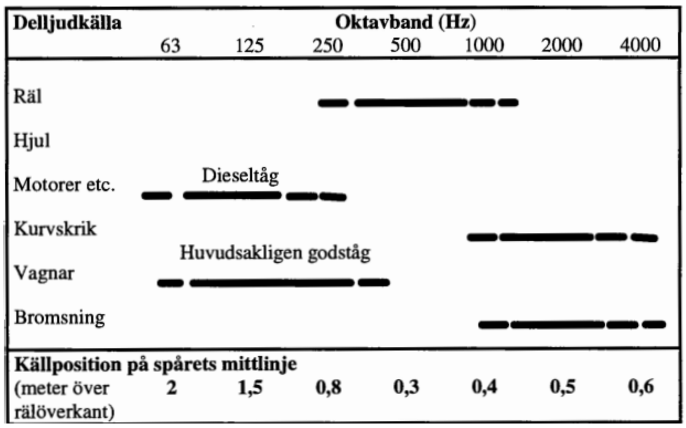

Figure 2.2: The rail source model of the Nord 96 report [2].

Partially based on the input data from the Nord 96 model, the Nord 2000 provide for a revised more detailed version shown in Table 2.1. Instead of positioning the source above the midpoint of the track the source is now placed above the rail closest to the receiver. If not stated otherwise the sources used are considered equal in strength.

	Height above top of rail (m)	**Frequency range (Hz)**	**Horizontal location**
Source 1 Wheel/Rail	0.01	200 - 10000	Evenly distributed along the train
Source 2 Wheel/Rail	0.35	200 - 10000	Evenly distributed along the train
Source 3 Wheel/Rail	0.70	200 - 10000	Evenly distributed along the train
Source 4 Engine	2.5	25 - 160	Centre of engine openings

Table 2.1: Default model parameters of the Nord 2000 rail source model in [6]. The engine noise is relevant for diesel driven locomotives only. The aerodynamic noise is omitted from this model as the cases are highly individual and often not relevant on Nordic tracks due to speed limits[3] of today. This might change in the future due to development of high speed rail infrastructure. Often frequencies below 50 Hz and above 5000 Hz can be neglected.

As mentioned in section 2.2.1.1 the effect of horizontal and vertical directivity is accounted for in the Nord 2000 source model. It can be calculated by

$$\Delta L(\varphi) = 10 \lg \left(0,15 + 0,85 \sin^2(\varphi)\right) + 2 \text{ (dB)} \tag{2.8}$$

where φ is the angle to the normal to the train/source. The directivity is of little importance when calculating equivalent levels, but can become important when calculating the values of individual point sources and is therefore mentioned here. The vertical directivity is deemed redundant in [6] and is omitted.

Another important thing to consider when modelling the train as a source is the relative distribution of energy between the different sub-sources. In [24] X. Zhang studies the energy distribution of a X2000-model train, this is later tuned in [3]. It shows that the distribution have a clear correlation to frequency and speed. The aerodynamic noise contribute to the total sound pressure up to 500 Hz for speeds below 200 km/h, if the speed increases to above 200 km/h the contribution extends to 1 kHz and above.

For example some cases of the energy distribution for different speeds, as suggested in [3], are compared in Figure 2.3. One notable thing is the clearly dominant sound power level from the boogie noise at frequencies below 315 Hz. This high level is most likely due to the very noisy cooling fans on the X2000 boogie and would as such not be as present in other train models. By that assumption the contributions in the region below 315 Hz is dominated by the Rail/Wheel. Above 315 Hz the wheel radiation is significant and at 2 kHz the wheel is the largest contributing source. When the speed increases it is clear that the aerodynamic sources becomes increasingly significant and at 200 km/h they become the dominating source up to about 800 Hz.

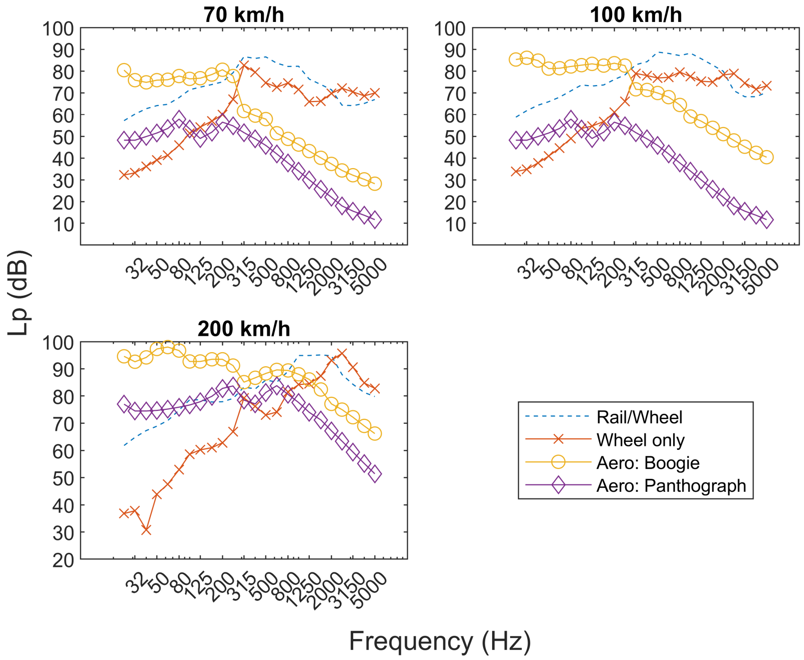

Figure 2.3: Sound power generated by a X2000 train at 70 km/h, 100 km/h and 200 km/h [3].

2.4.2 Geometrical considerations

Taking the scope of the thesis in consideration, the obvious choice of basis for the geometry of the train and rail is the active Swedish standards. To be allowed to traffic the railways in Sweden STA have a certain set of so called load profiles that trains have to follow. These profiles are specified in [4] and in this case the dynamic reference profile presented in Figure 2.4 is used.

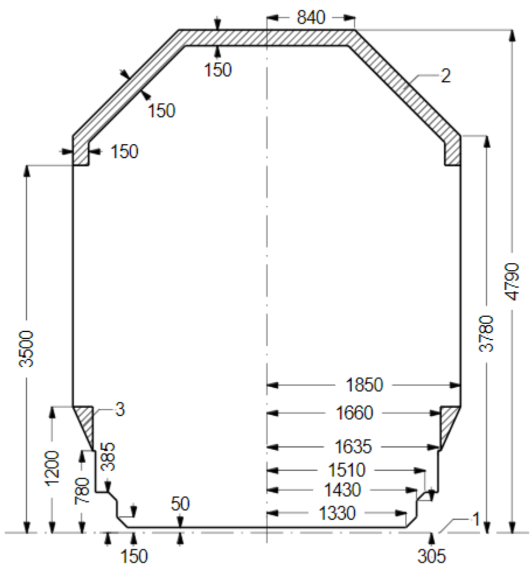

Figure 2.4: Dynamic reference profile SEa. Dimensions are in mm [4].

In reference to this and Swedish safety standards [13][12] any NRD of significant height must be placed at least 1.7 m from the center of the track. One type of LHNS available in Sweden is S-block, the dimensions of which is presented in Figure 2.5. The main track gauge in Sweden is 1435 mm [25] and it will be the dimension used in the modelling process.

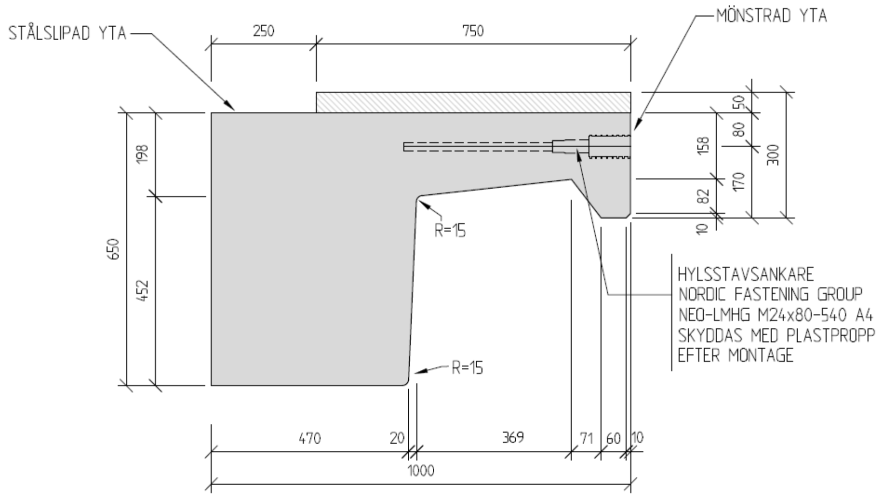

Figure 2.5: Dimensions in mm of a LHNS provided by Z-bloc Norden [5]. The effective height of the screen is 1 m and it is purposefully placed in such a way that the top of the screen is 0.73 m above the top of the rail. The upper 750 mm part of the screen is made out of an absorbent material called "Vitrumite" [1].

3

BEM - Theory and Code-Implementation

In this chapter the basic principles of BEM-theory is presented with illustrations of how it is implemented in the code. The aim is to, along side of the complicated mathematics, provide a more intuitive approach and by doing so enable understanding for a wider reader-base.

3.1 The Kirchhoff Helmholtz Integral (KHI)

A train situated above rail and ballast with an implemented noise screen can, if studied from a cross-section perspective, look something like the case shown in Figure 3.1. The surfaces of both the train $\mathcal{S}_T$, the ballast and the screen $\mathcal{S}_{BS}$ build a set of points $\mathcal{S}_{surf}$ which are enclosing the set of points $\mathcal{V}_{BST}$ consisting of the volumes $\mathcal{V}_{BS}$ and $\mathcal{V}_T$ respectively within in volume $\mathcal{V}_{free}$.

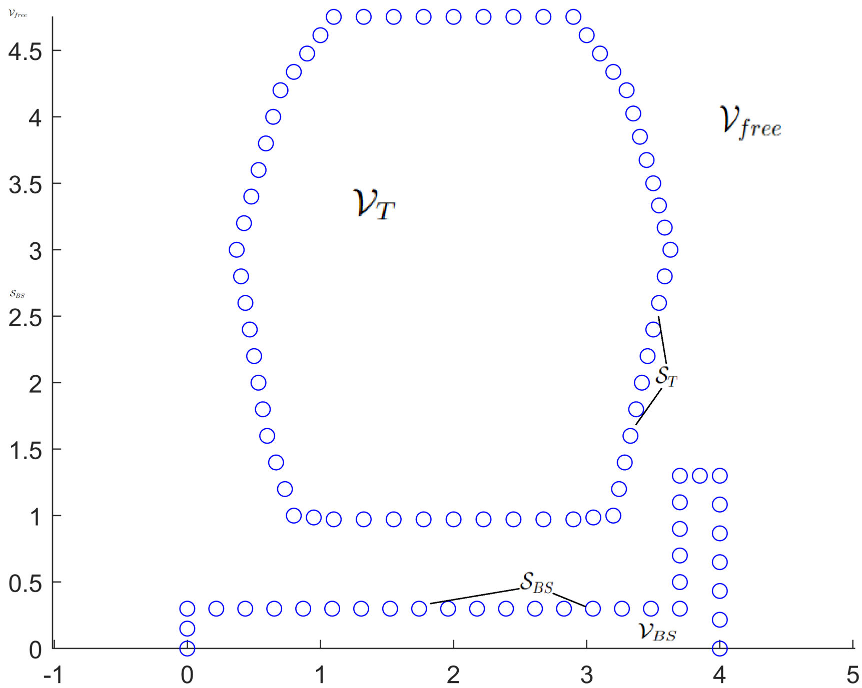

Figure 3.1: A rough estimate of the cross section of a X60 train discretised into segments.

If a source q_0 is placed somewhere inside of $\mathcal{V}_{free}$, see Figure 3.1, then the pressure at any point x_r inside of $\mathcal{V}_{free}$ caused by the direct pressure and the pressures reflected of the surfaces can be calculated by

$$\left.\begin{array}{c}\text{If } x_r \in \mathcal{V}_{free} \text{ and } \notin S_{surf}, 1\\ \text{If } x_r \in \mathcal{S}_{surf}, \frac{1}{2}\\ \text{else}, 0\end{array}\right\} \cdot p\left(x_r\right) = \underbrace{\frac{1}{4\pi}\int_V \frac{e^{-jkR}}{R} q_0 \, dV}_{\text{Volume source } = p_{q_0}} \ldots$$
$$+\frac{1}{4\pi}\int_S \frac{e^{-jkR}}{R} p_s \left(\underbrace{jk\beta}_{\text{Monopole layer}} - \underbrace{\left(jk + \frac{1}{R}\right)\left(\vec{e}_R \bullet \vec{n}_S\right)}_{\text{Dipole layer}} \right) dS \tag{3.1}$$

where k is the wavenumber, R is the source-receiver distance, q_0 is some source with a shape function, p_s is the pressure on the surface of $\mathcal{S}_{surf}$, β is some normalised impedance[1], $\vec{e}_R$ is a unit vector for the source-receiver direction and $\vec{n}_S$ is the unit vector normal to the surface. The derivation of this integral can be found in appendix A.

3.2 Solving the KHI with 2D-BEM

The KHI can be solved by moving the receiver x_r to $\mathcal{S}_{surf}$ and solving for the pressure on the surface. Equation 3.1 can then be written as

$$\frac{1}{2}p(x_r|x_s) = p_{q_0} + \frac{1}{4\pi}\int_S p_s \frac{e^{-jkR}}{R}\left(jk\beta - \left(jk + \frac{1}{R}\right)\left(\vec{e}_R \bullet \vec{n}_S\right)\right) dS \tag{3.2}$$

The problem can be transported to the numerical domain by discretisation of the surface into $S_N = \{1, 2, 3 \ldots N\}$ smaller elements and 3.2 can be written as

$$\frac{1}{2}p_{s,i} = p_{q_0,i} - \sum_{j=1}^{N} p_{s,j} \underbrace{\frac{e^{-jkR_j}}{R_j}\left(jk\beta - \left(jk + \frac{1}{R_j}\right)\left(\vec{e}_{R_j} \bullet \vec{n}_{S_j}\right)\right)\Delta S_j}_{\vec{r}_{i,j}} \tag{3.3}$$

where p_i is the pressure at the i:th element on the surface, $p_{s,j}$ is the contribution to that pressure from every other element on the surface and $p_{0,i}$ is the pressure from the source, and reformulated to solve for the pressure on the surface

$$p_{q_0,i} = \left[\frac{1}{2} + \sum_{j=1}^{N} \frac{e^{-jkR_j}}{R_j}\vec{r}_{i,j}\right] p_{r,i} \tag{3.4}$$

and with matrix formulation $Ax = B$

$$\underbrace{\begin{bmatrix} p_{q_0,1} \\ p_{q_0,2} \\ . \\ . \\ p_{q_0,i} \end{bmatrix}}_{B} = \underbrace{\begin{bmatrix} \frac{1}{2}\vec{r}_{1,1} & \vec{r}_{1,2} & \cdots & \vec{r}_{1,j} \\ \vec{r}_{2,1} & \frac{1}{2}\vec{r}_{2,2} & & \vdots \\ \vdots & & \ddots & \\ \vec{r}_{i,1} & \ldots & & \frac{1}{2}\vec{r}_{i,j} \end{bmatrix}}_{A} \cdot \underbrace{\begin{bmatrix} p_{s,1} \\ p_{s,2} \\ . \\ . \\ p_{s,j} \end{bmatrix}}_{x} \tag{3.5}$$

[1] This can be any model that would fit the purpose of the project. In this case the Slit-Pore model is used because both the Vitrumite in the S-block and the train ballast is porous

the pressure on the surface can be solved with matrix inversion $x = A \times B^{-1}$. When the pressure on the surface is known the contribution of each individual element can be summed at some receiver point $x_r \in V_{free}$ by

$$p_{tot}(x_r) = p_{q_0}(x_r) - \sum_{j=1}^{N} p_{s,j} \frac{e^{-jkR_j}}{R_j} \left(jk\beta - \left(jk + \frac{1}{R_j} \right) (\vec{e}_{R_j} \bullet \vec{n}_{S_j}) \right) \Delta S_j \tag{3.6}$$

In short this summation describes the total pressure caused by both direct and scattered sound from any object in the volume $\mathcal{V}_{free}$ at the receiver x_r.

To avoid problems generated by singularities such as unwanted resonances in the volumes outside the volume of interest so called chief-points should be added to the volumes. These points over-determine equation 3.6 with points where the pressure is forced to zero and eliminating any resonances inside of the structure(s). In the model the amount of points added to the structure will set to be a specific amount per wavelength fitting in the largest size of the geometries by

$$N_{ch} = \frac{d_{max} * C_{ppw}}{c0/f} \tag{3.7}$$

where d_{max} is the largest size in the model geometries, C_{ppw} is the amount of points per wavelength fitting in the structure, $c0$ is the speed of sound and f is the frequency.

3.3 2.5D Geometry

As mentioned in section 2, modelling in the 2D-plane[2] assumes the sources to be homogeneous over the y-axis or in the case of a train, over the length of the train in the direction of travel. While some studies has shown that there can be good agreement between 2D and 3D cases, information such as phase shifts and individuality of the sources gets lost [18].

A better approximation would be an infinite incoherent line-source consisting of an array of point sources spaced individually over length of the train. A good example of this can be found in the Nord 2000 rail propagation model [6]. To make simulations of this possible by standard means the problem would have to be extended to the 3D-plane. However because BEM discretises the radiating surfaces the amount of solutions needed in the 3D plane increases exponentially in relation to the 2D plane [19]. To solve this D. Duhamel propose that a fourier type integration where the 2D solution produced by equation 3.6 is assumed to be homogenous in the y-direction, the 3D pressure p_{3D} as a function of the wave number can then be estimated by

$$p_{3D}(x, y, z, k(v)) = \frac{1}{2\pi} \int_{-\infty}^{\infty} e^{i\alpha y} p_{2D}\left(x, z, \sqrt{k^2(v) - \alpha^2}\right) \, d\alpha \text{ (Pa)} \tag{3.8}$$

where y is the source-receiver distance in the y-plane, p_{2D} is the 2D pressure at (x, z) calculated using equation 3.6 as a function of some real or imaginary wavenumber $\sqrt{k^2(\nu) - \alpha^2}$.

[2] XZ-plane

To get the equivalent levels as the train passes an angle dependency can be applied to the source-receiver distance y by

$$y(\Theta) = y_0 \tan \frac{\Theta\pi}{180} \ (m) \tag{3.9}$$

where y_0 is the source receiver distance on the XZ-plane and Θ is the angle of the sources XYZ-position in relation to XZ-plane.

3.4 2D MATLAB Implementation

In the Figures 3.2 - 3.5 an illustrative example of how the model is implementing discretisation to be able to solve equation 3.6.

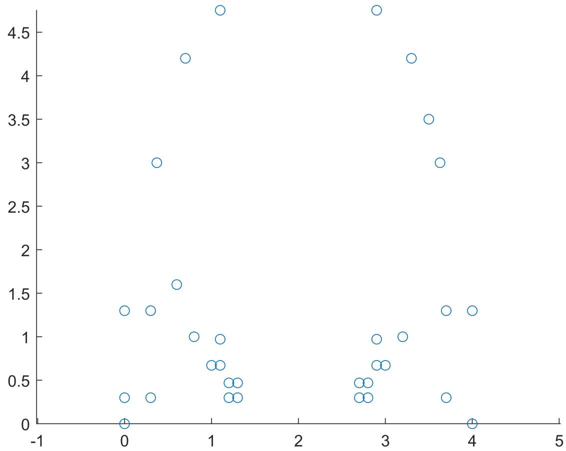

Figure 3.2: A set of coordinates define the outline of the structures.

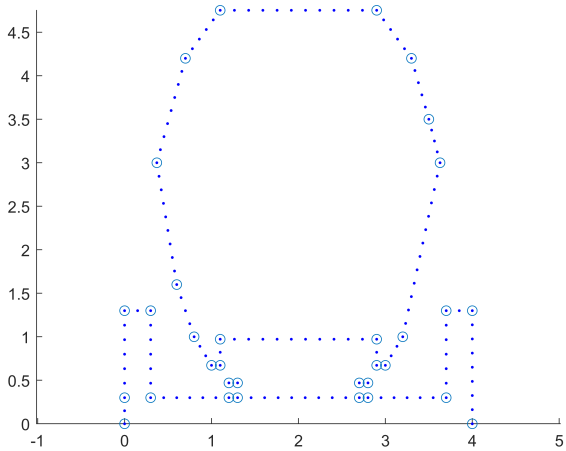

Figure 3.3: The surfaces are defined and discretised. The resulting amount of segments are depending on the spatial resolution N_s and frequency. Here arbitrary values are used for the sake of illustration.

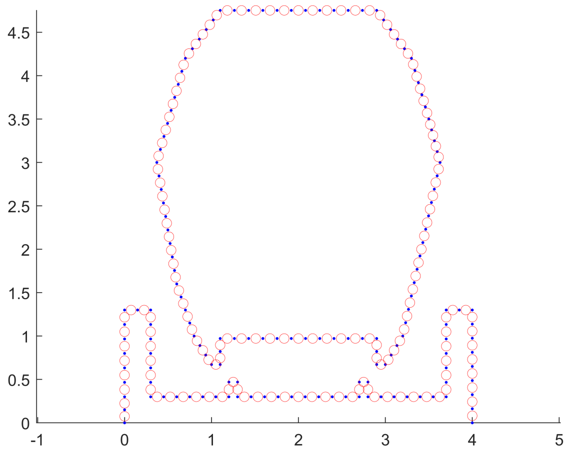

Figure 3.4: The discretised version of the monopole layer mentioned in equation 3.1 is added.

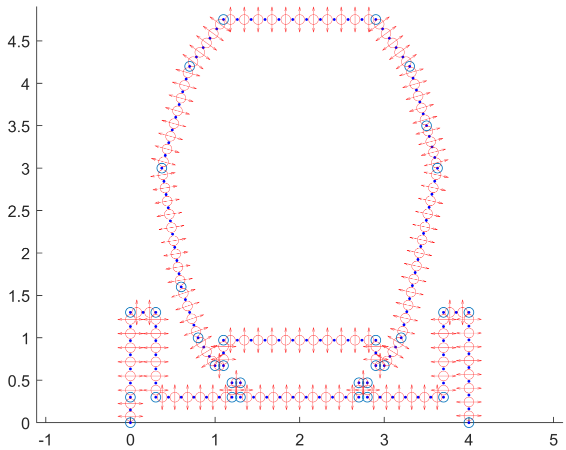

Figure 3.5: The discretised version of the dipole layer mentioned in equation 3.1 is added.

To account for the impedance of specific segments, β in equation 3.6 can be defined as some impedance model. In this case impedance is applied at the red X:s in Figure 3.6. Furthermore, to avoid the additional computational load caused by the discretisation of the ground, it can be assumed hard and a mirror plane can be introduced as in Figure 3.6. The final 2D-pressure at x_r can be calculated by equation 3.6.

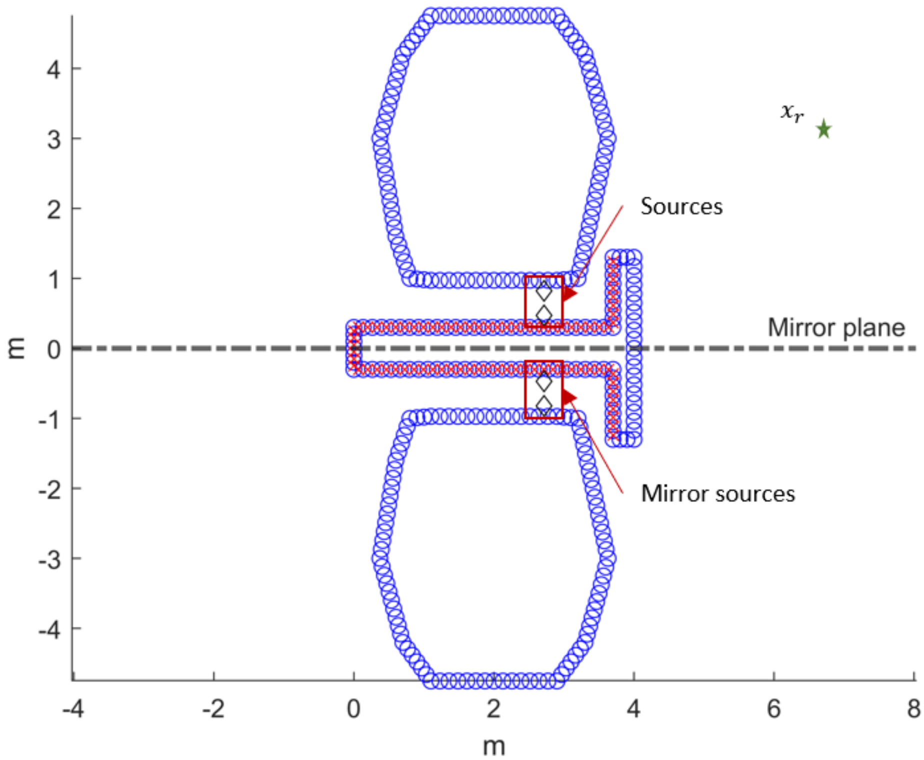

Figure 3.6: An example of a model geometry mirrored about the mirror plane. The green star represents some receiver location x_r and the black diamonds represents the original and mirrored sources.

3.5 Post-Processing

To get the final results based on the 2.5D pressure calculations some post-processing of the data is required. To properly simulate the sound field a weighting based of the sound power distribution in [3] for a train moving at 70 km/h converted to pressure is made. The weighting for both the rail(low) and wheel(high) source is calculated as the relative contribution of power

$$R_{Ew}(f) = \frac{W_{0,\mathrm{rail}}(f)}{W_{0,\mathrm{rail}}(f) + W_{0,\mathrm{wheel}}(f)} \; (-) \tag{3.10}$$

and

$$W_{Ew}(f) = \frac{W_{0,\mathrm{wheel}}(f)}{W_{0,\mathrm{rail}}(f) + W_{0,\mathrm{wheel}}(f)} \; (-) \tag{3.11}$$

A weighting is calculated using the data presented in Figure 2.3 of a train travelling at 70 km/h. The resulting ratios are presented in Figure 3.7.

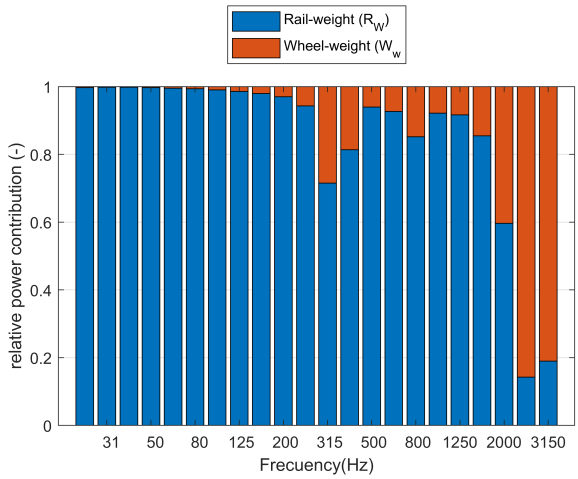

Figure 3.7: Calculated weights of a train travelling at 70 km/h based on the research in [3].

Now the total sound energy from both sources of the train can be expressed as

$$|p_{0,Ew}(f)|^2 = |p_{0,\mathrm{rail}}(f)|^2 R_w(f) + |p_{0,\mathrm{wheel}}(f)|^2 W_w(f) \; (\mathrm{Pa}) \tag{3.12}$$

where $p_{0,rail/wheel}$ is the simulated pressure from each of the sources.

As the validation data available is in both equivalent and maximum levels, two different sets of data is needed. The equivalent, average pressure level over the angle dependency for each frequency is calculated by

$$L_{p,Ew,Deq} = 10 \times \log 10\Big(\frac{1}{n} \sum_{n}^{Nd} |p_{0,Ew,n}|^2\Big) \; (\mathrm{dB}) \tag{3.13}$$

where n is the index of each angle Θ, N_d is the total amount of angles in p_0.
The maximum pressure level $L_{p,0^\circ}$ is assumed to be where the source receiver distance is as short as possible i.e. at $\Theta = 0^\circ$ and no average is made. At this point there

is no angle dependency thus no directivity is considered. The reference pressure is omitted as it will be divided away in the calculation of the IL, which is done by subtracting the post-processed results of the each case simulated without and with the LHNS.

$$IL_{Ew,Deq} = L_{p,Ew,Deq,without} - L_{p,Ew,Deq,with} \text{ (dB)} \tag{3.14}$$

for the angle equivalent values and

$$IL_{Ew,0°} = L_{p,Ew,0°,without} - L_{p,Ew,0°,with} \text{ (dB)} \tag{3.15}$$

for the maximum pressure values. To calculate the total average A - weighted insertion loss for both the angle equivalent case and the maximum, the average total pressure with and without screen is calculated by

$$Lp_{Aeq,Ew,Deq,with/without} = 10 \times \log 10\Big(\frac{1}{N_f}\sum_{m}^{Nf} 10^{0.1 \cdot L_{p,Ew,Deq,with/without,m}}\Big) \text{ (dBA)} \tag{3.16}$$

and

$$Lp_{Aeq,Ew,0°,with/without} = 10 \times \log 10\Big(\frac{1}{N_f}\sum_{m}^{Nf} 10^{0.1 \cdot L_{p,Ew,0°,with/without,m}}\Big) \text{ (dBA)} \tag{3.17}$$

where m is the index of each frequency in the spectrum and N_f is the total amount of frequency bands. The total average IL for both the angle equivalent and the maximum case is then calculated by

$$IL_{Aeq,Ew,Deq} = Lp_{Aeq,Ew,Deq,without} - Lp_{Aeq,Ew,Deq,with} \text{ (dBA)} \tag{3.18}$$

and

$$IL_{Aeq,Ew,0°} = Lp_{Aeq,Ew,0°,without} - Lp_{Aeq,Ew,0°,with} \text{ (dBA)} \tag{3.19}$$

4

Setup, Simulations and Validations

In this chapter the setup of the simulated cases are presented in more detail. Furthermore the data that is used to compare and validate the results of the simulations are presented.

4.1 Setup and Simulations

To get a good and diverse estimate of the general IL when implementing a LHNS, three different geometrical estimations of a train body are made, see Figure 4.1, 4.3 and 4.4. Figure 4.1 is roughly modelled after the X60 commuter trail model using the SEa load profile and the dimensions in [26] as reference. Figure 4.3 is a very basic estimation of an empty timber- or industrial-wagon, again modelled using the SEa as reference. Figure 4.4 is a ballast and a screen, without a wagon.

The LHNS is placed so that the top of the screen is 0.73 m above the top of the rail and so that the part facing the source is 1.7 m from the rail center. The source positions used are marked as red diamonds. Segments with added admittance are marked with a red X.

To be able to estimate the IL of the LHNS each case is simulated with and without screen, see Figure 4.2. In accordance to the source model from Nord 2000, table 2.1, the source location is above the rail closest to the receiver at 0.01 m, 0.35 m and 0.70 m above the top of the rail. In the case using the X60-model the high wheel source is not available due to the boogie.

The receiver locations are placed at three horizontal position $x = [7.5, 27, 35]$m from midpoint of the track. At $x = 7.5\,\mathrm{m}$ five receiver positions centred around $z = 1.2\,\mathrm{m}$ above the top of the rail are placed. At $x = 27\,\mathrm{m}$ and $x = 35\,\mathrm{m}$ five receiver positions centred around $z = 3.5\,\mathrm{m}$ above the top of the rail are placed. These positions correspond to the measurement positions of the validation data presented in section 4.2.

Because of limitations in the BEM-implementation only one type of admittance can be added to the surfaces at the same time. Therefore it was decided to use the admittance of the ballast on every segment with added admittance.

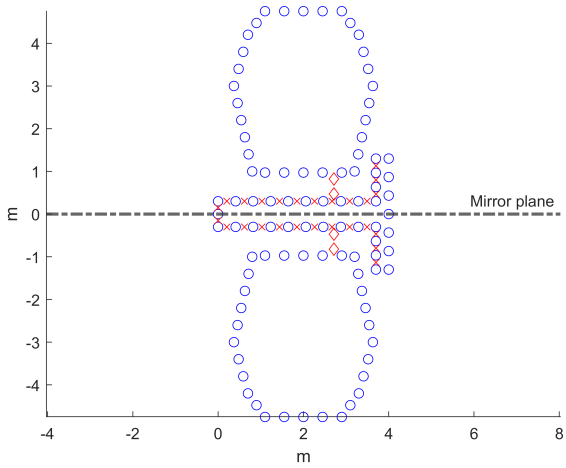

Figure 4.1: Model based roughly of a X60-commuter train above a ballast with a single LHNS.

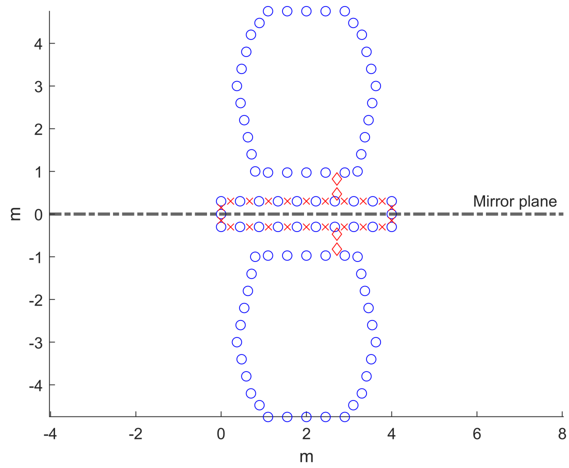

Figure 4.2: The X60 model case without screen.

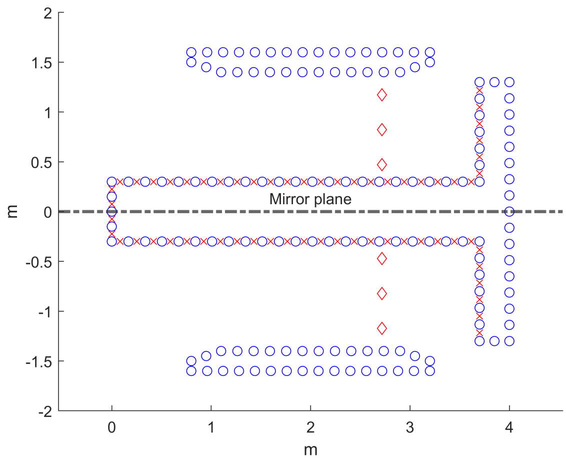

Figure 4.3: Model based roughly of an empty timber wagon above a ballast with a single LHNS.

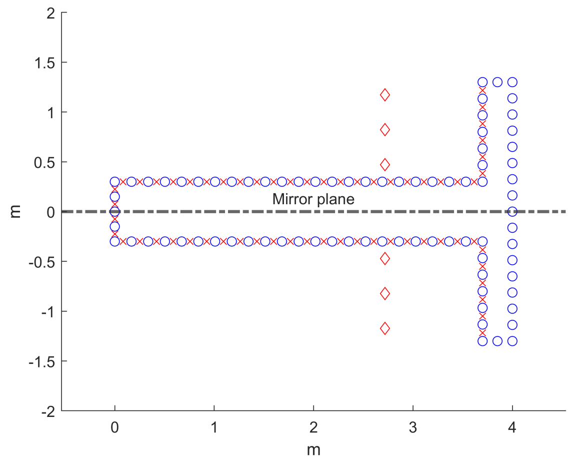

Figure 4.4: Model based roughly of a ballast with a single LHNS.

4.1.1 Tuning the Model

With the necessary geometrical considerations specified the BEM-implementation parameters need to be tuned to get as accurate results as possible in relation to computation time. Because of the relatively large geometrical designs the full spectrum of third-octave bands up to 5000 Hz was not possible. Instead the limit was set at 3150 Hz. To achieve as accurate results as possible it is important to set the spatial resolution fine enough. However a finer resolution in turn causes a significant increase in computation times. Therefore a good balance have to be found and N_s, see Figure 3.3 have to be tuned accordingly.

If too many chief points are added to the structure relative the amount of discretised segments they can take precedence and cause erroneous pressure values. Therefore the amount added by equation 3.7 have to be tuned in accordance to the model. The results of this tuning process can be found in Appendix B. Sub-

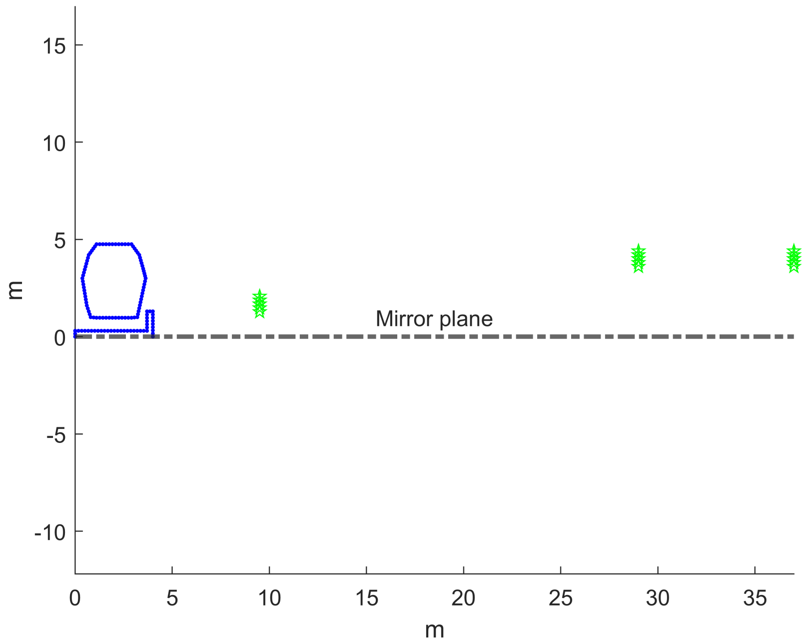

Figure 4.5: Receiver placements used. From left to right they correspond to reference measurements from Quiet City, Skogås (Nya Östra Skolan), Saltsjöbanan.

sequent of tuning the numerical parameters a comparison between the Hamet- and Slit-Pore impedance model was made. The best fit to the measurement-data could be achieved using the Slit-Pore model and is therefore used in the modelling. As no data is available on the ballast a process of trail and error was done to find the best fit to the reference data. This trail and error process had a starting point using the parameters for slit-pore and hamet model in [27] and [28]. In the end a flow resistivity of 2200 $\mathrm{Ns/m^4}$ and a porosity of 0.491 is used. If the reader has further interest in the origins of these parameters, as well as additional information regarding the impedance model, he/she is urged to read the research in [28] and [27].

4.2 Validation Data

To validate the results and tune the model, information from three different reports was compiled and made to fit the parameters of this thesis. The reports measures the sound pressure levels before and after implementing a LHNS. If the data available was not specified in a third octave band it was extracted by utilising a software called "Engauge Digitizer" [29]. This software works by:

1. Importing the image of a graph
2. Defining the values of the x - and y - axis
3. Mark the wanted data-points in the graph using the mouse cursor
4. Exporting the values of these data-points

4.2.1 Quiet City

The project Q-City carried out measurements on a track between Kungsängen and Västerås where Z-bloc Nordens LHNS was used [7].

The receiver locations used for the measurements without an emergency door is presented in Table 4.1

	Distance from track center (m)	**Height above top of the rail (m)**	**In accorance to:**
Mic 3 (with LHNS)	7.5	1.2	SSEN-ISO3095
Mic 4 (w.o LHNS)	7.5	1.2	SSEN-ISO3095
Mic 5 (w.o LHNS)	10	2.0	Nord 2000

Table 4.1: The receiver locations in [7] used for the extracted data.

The extracted IL on the spectrum 31 Hz to 5 kHz is presented in Table 4.2.

Frequency (Hz)	**25**	**31**	**41**	**50**	**63**	**80**	**100**	**125**	**160**	**200**	**250**	**315**	**400**	**500**	**630**	**800**	**1000**	**1250**	**1600**	**2000**	**2500**	**3150**
X60 IL (dB)	0	0	0	0	0.83	1.79	1.26	2.14	7.01	8.65	4.55	7.77	8.88	6.95	7.88	12.09	7.12	7.44	6.12	5.50	6.16	6.39
Goods IL (dB)	0	1.30	0.02	0.04	1.15	1.55	0.22	0.62	2.06	3.92	2.74	2.79	3.06	2.00	3.76	4.58	3.32	4.07	4.41	3.89	4.22	4.19

Table 4.2: IL calculated with and without screen in the Quiet City report [7]. Several different train types are recorded. The different sets of measurements are carried out in accordance to specifications of both SS-EN ISO3095:2013 and Nord 2000.

4.2.2 Saltsjöbanan

By request of AB Storstockholms Lokaltrafik(SL), ÅF Sound and Vibrations, to date called Efterklang, carried out control measurements at an installation location of LHNS [8]. The measurements with and without noise screen were carried out at 2012-05-23 and 2013-11-13 respectively.

The reference measurement position is located on the facade of a house on Lilllängsvägen 43. The distance from the track is approximately 27 m and the height above ground is by ocular inspection estimated to be between 2.5 m and 4 m. The extracted data is presented in table 4.3

Frequency (Hz)	**25**	**31**	**41**	**50**	**63**	**80**	**100**	**125**	**160**	**200**	**250**	**315**	**400**	**500**	**630**	**800**	**1000**	**1250**	**1600**	**2000**	**2500**	**3150**
IL_{Lpmax} **(dB)**	-8.11	-9.32	-6.97	-4.09	-2.60	1.44	5.20	4.76	5.41	8.58	12.78	12.01	8.06	9.27	11.66	11.57	12.33	12.97	15.79	16.63	15.35	16.38

Table 4.3: IL based on the maximal recorded sound power levels in third octave bands from the report [8]. Before and after construction of the LHNS.

4.2.3 Nya Östra Skolan

Acoustic Control AB have by request of Huge Fastigheter made measurements on the sound power levels caused by the passing trains before and after construction of the School [9]. The before and after measurements were carried out in 2002 and 2005 respectively. The frequency spectrum data is presented in table 4.4.

Frequency (Hz)	**25**	**31**	**41**	**50**	**63**	**80**	**100**	**125**	**160**	**200**	**250**	**315**	**400**	**500**	**630**	**800**	**1000**	**1250**	**1600**	**2000**	**2500**	**3150**
Northbound IL_{Lpmax} **(dB)**	-3.0	2.1	-3.4	3.8	8.5	12.0	3.6	0.4	-1.2	3.1	7.3	7.5	8.3	7.6	7.4	16.6	14.6	12.6	12.1	12.4	14	14.7
Southbound IL_{Lpmax} **(dB)**	5.4	-0.4	1.3	-1.2	4.9	8.0	4.3	-3.1	-5.2	0.4	4.0	5.0	3.3	3.2	4.5	16.3	8.2	6.0	12.0	8.0	11.5	11.1

Table 4.4: IL based on the maximum recorded sound power level in third octave bands on northbound trains [9] before and after construction of the school and the LHNS.

5

Results

In this Chapter the results of the simulations made on the three cases described in Chapter 4 are presented.

The height of the source positions are (above the top the rail):

- Rail at 0.01 m
- Wheel Low at 0.35 m
- Wheel High at 0.70 m

In Figure 5.1 to Figure 5.21 the results of the simulations on the different train models are presented. In the leftmost (uneven numbered) figures results from both rail and wheel sources are presented along side the resulting energy distribution weighted IL. In the rightmost (even numbered) figures the same weighted IL is presented along side the different reference measurements. The variables have been color coded to stay the same

5.1 Case 1: X60 - SLs Commuter Trains

5.1.1 Quiet City Reference Positions

In Figure 5.2 note the clear divergence above 800 Hz.

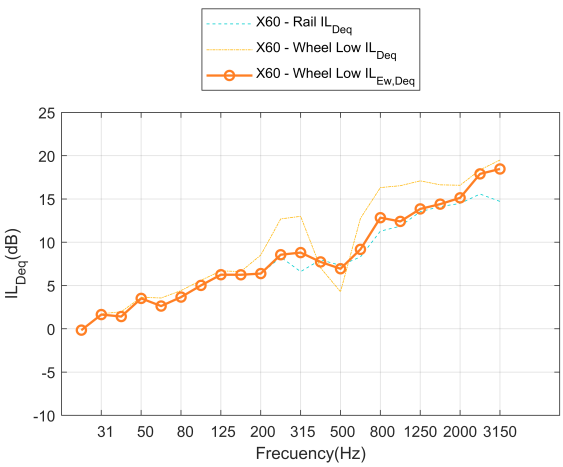

Figure 5.1: Simulated IL of the X60-model at receiver positions corresponding to the Quiet City measurements.

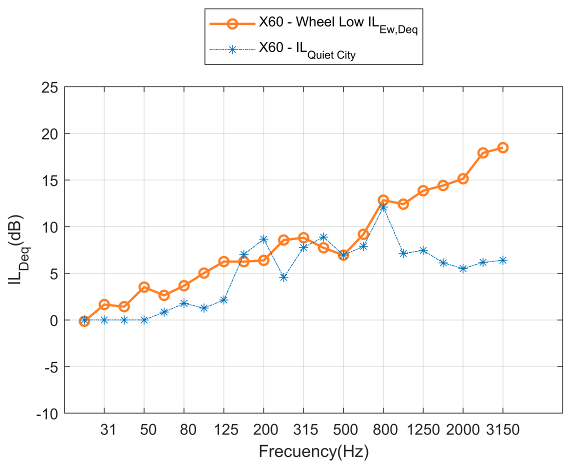

Figure 5.2: The total source weighted IL of the X60-model compared to the Quiet City measurements of a X60-train.

5.1.2 Nya Östra Reference Positions

In Figure 5.4 note how there is a common trend between the simulations and the references, with a slight shift in frequency of the peaks.

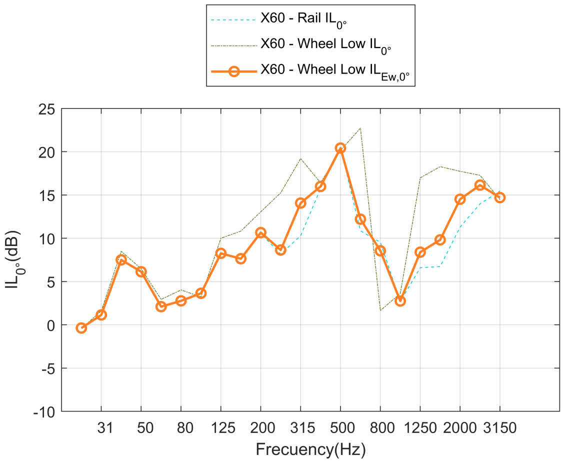

Figure 5.3: Simulated IL of the X60-model at receiver positions corresponding to the Nya Östra measurements.

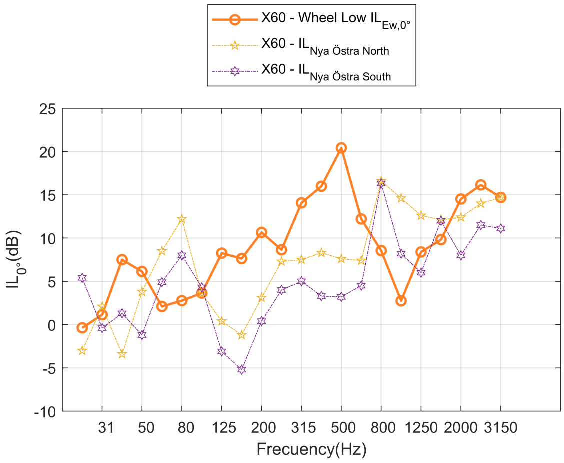

Figure 5.4: The total source weighted IL of the X60-model compared to the Nya Östra measurements.

5.1.3 Saltsjöbanan Reference Positions

In Figure 5.6 note the similarities in the region of 80 Hz to 315 Hz.

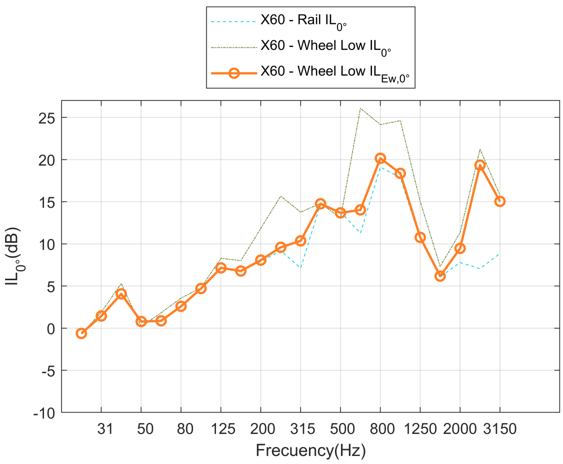

Figure 5.5: Simulated IL of the X60-model at receiver positions corresponding to the Saltsjöbanan measurements.

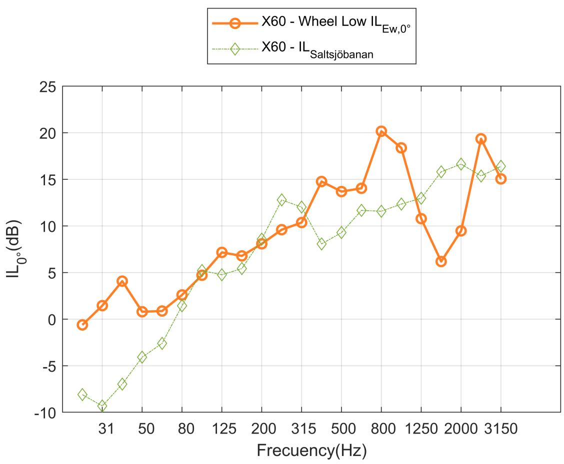

Figure 5.6: The total source weighted IL of the X60-model compared to the Saltsjöbanan measurements.

In Figure 5.1, 5.3 and 5.5 it can be noted that the IL of the wheel source show a generally higher level than the rail source.

5.1.4 X60: A - Weighted Total

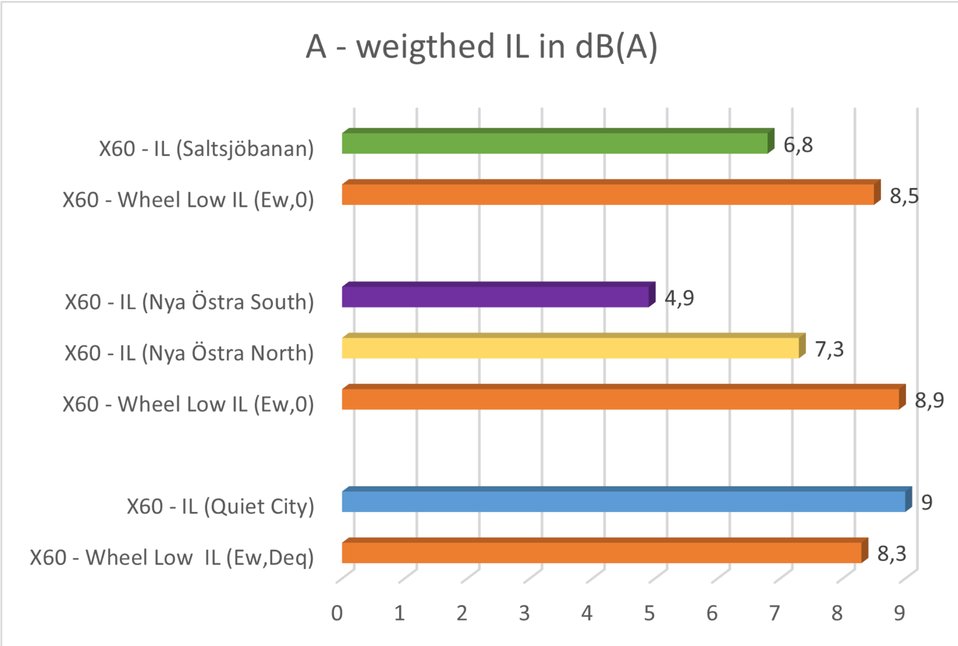

Figure 5.7: A - weighted IL of the different X60-model receivers in comparison to their respective reference measurements.

5.2 Case 2: Industrial Wagon

5.2.1 Quiet city reference positions

Note in Figure 5.9 note the significant difference to the reference measurements of the goods wagon.

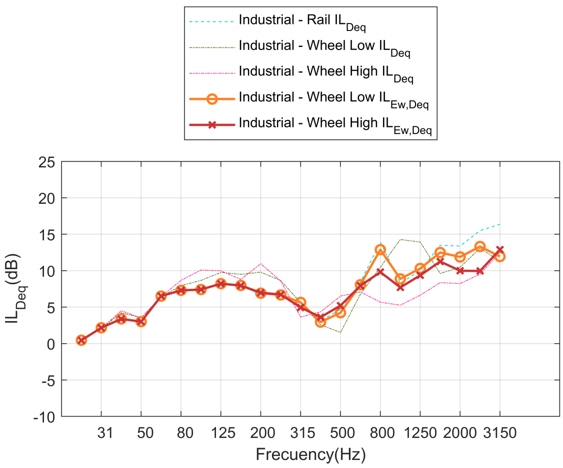

Figure 5.8: Simulated IL of the Industrial-model at receiver positions corresponding to the Quiet City measurements.

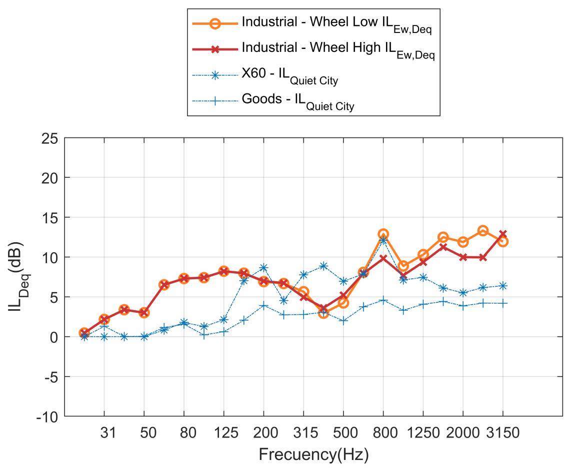

Figure 5.9: The total source weighted IL of the Industrial-model compared to the Quiet City measurements of a X60- and Goods-train.

5.2.2 Nya Östra Reference Positions

In Figure 5.10 and 5.11, not the large peak at 500 Hz. Note the similarities with Figure 5.4.

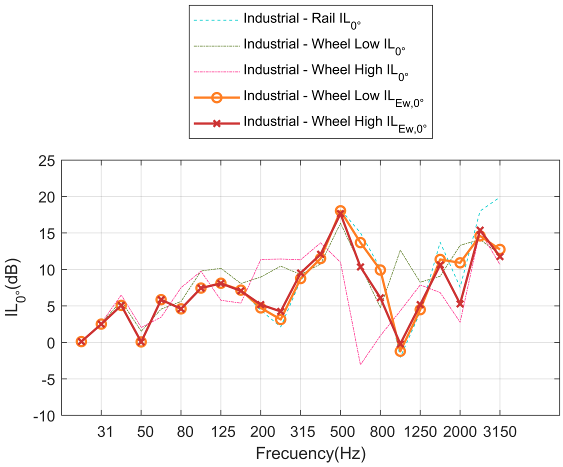

Figure 5.10: Simulated IL of the Industrial-model at receiver positions corresponding to the Nya Östra measurements.

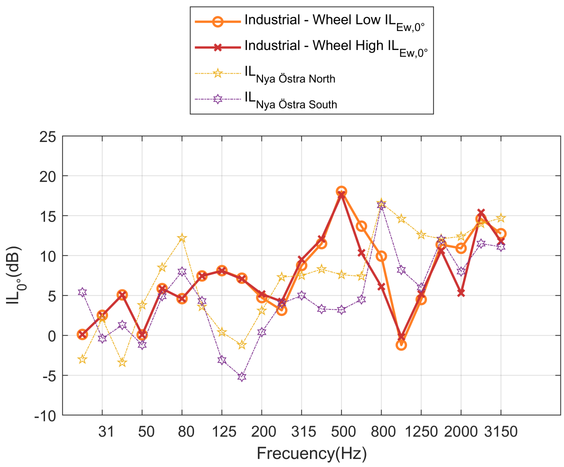

Figure 5.11: The total source weighted IL of the Industrial-model compared to the Nya Östra measurements.

5.2.3 Saltsjöbanan Reference Positions

In Figure 5.13 note the peak at 250 Hz.

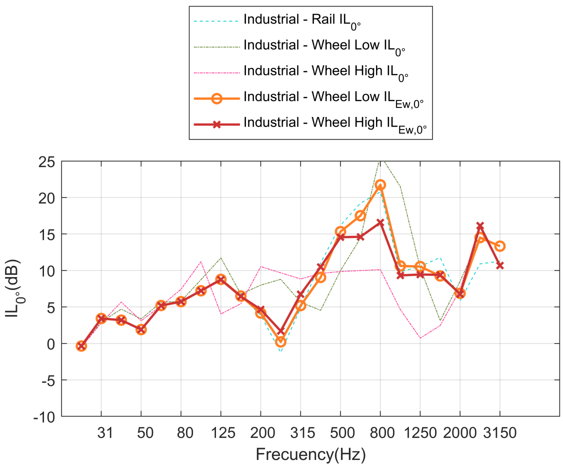

Figure 5.12: Simulated IL of the Industrial-model at receiver positions corresponding to the Saltsjöbanan measurements.

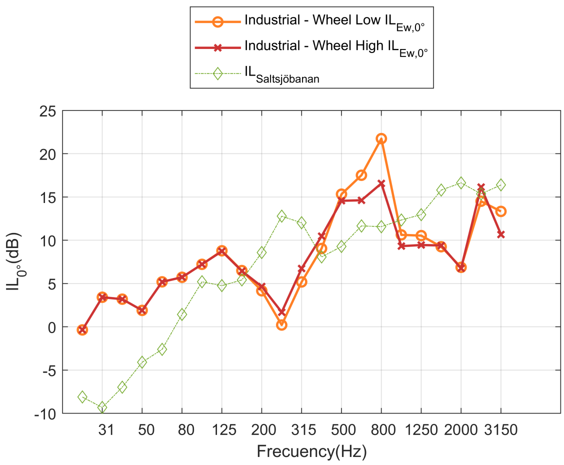

Figure 5.13: The total source weighted IL of the Industrial-model compared to the Saltsjöbanan measurements.

In Figure 5.8, 5.10 and 5.12 note the significantly lower levels of the high wheel source. Also note the effect this has on the weighted IL.

5.2.4 Industrial: A - Weighted Total

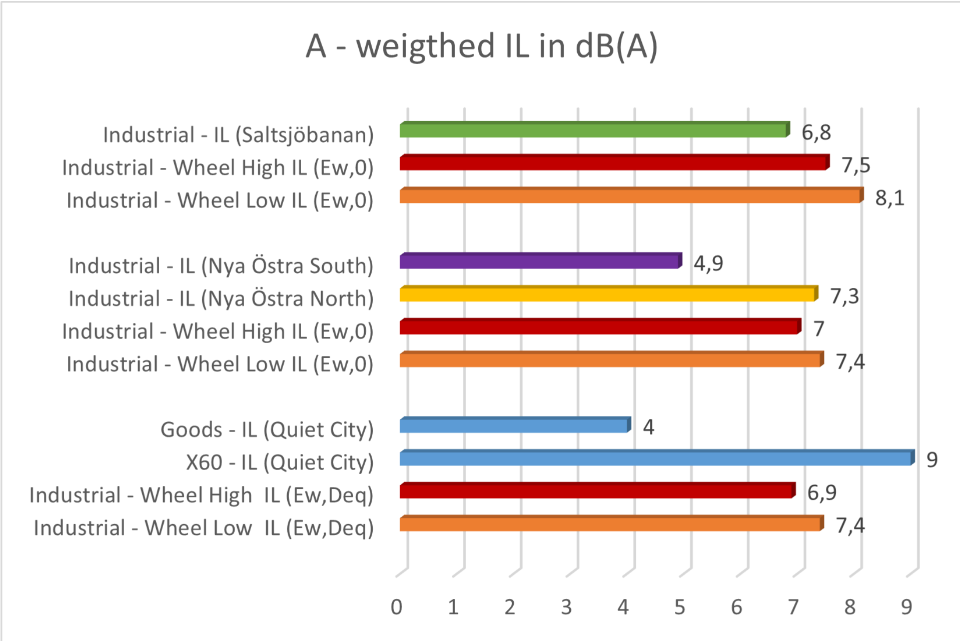

Figure 5.14: A - weighted IL of the different Industrial-model receivers in comparison to their respective reference measurements.

5.3 Case 3 - No Wagon

5.3.1 Quiet City Reference Positions

In Figure 5.16 not the similarities with Figure 5.2. Also note how the high wheel source affect the level above 800 Hz.

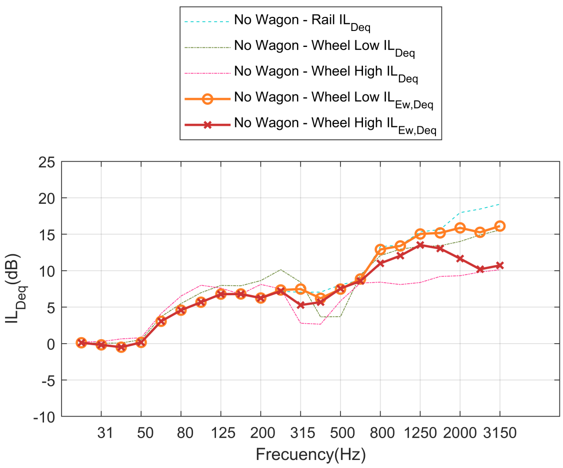

Figure 5.15: Simulated IL of the case without wagon at receiver positions corresponding to the Quiet City measurements.

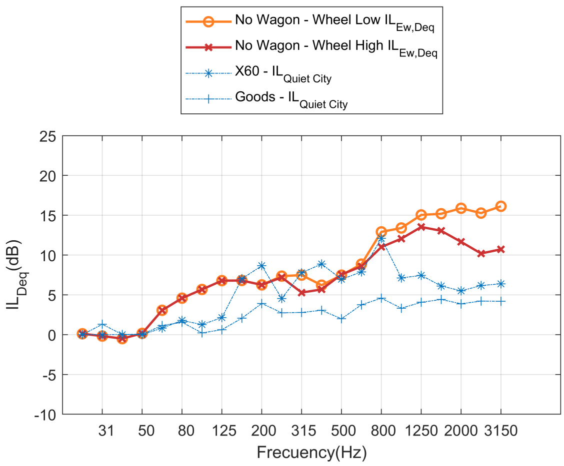

Figure 5.16: The total source weighted IL of the case without wagon compared to the Quiet City measurements of a X60- and Goods-train.

5.3.2 Nya Östra Reference Positions

In Figure 5.18 a common trend between the simulations and the reference values can be noted, though shifted in frequency. The behaviour is similar to the same reference position in both case 1 and case 2 but a more pronounced peak at 500 Hz

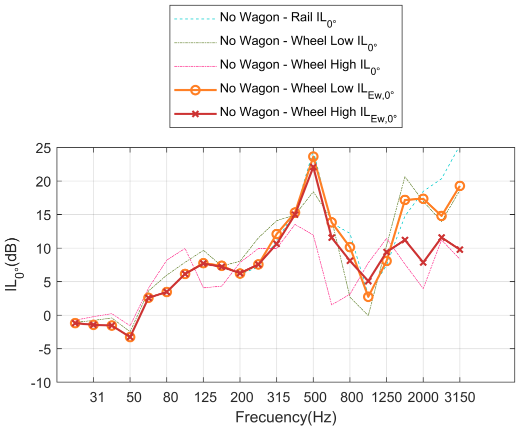

Figure 5.17: Simulated IL of the case without wagon at receiver positions corresponding to the Nya Östra measurements.

Figure 5.18: The total source weighted IL of the case without wagon compared to the Nya Östra measurements.

5.3.3 Saltsjöbanan Reference Positions

In Figure 5.20 a decent fit to the reference measurements can be noted in the region of 50 Hz to 315 Hz. Significant fluctuations about the level of the reference can be noted.

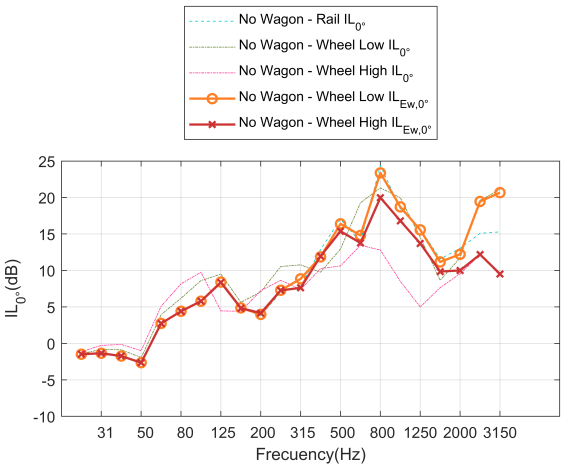

Figure 5.19: Simulated IL of the case without wagon at receiver positions corresponding to the Saltsjöbanan measurements.

Figure 5.20: The total source weighted IL of the case without wagon compared to the Saltsjöbanan measurements.

In Figure 5.15, 5.17 and 5.19, again the levels of the high wheel source is in general significantly lower. Note how this affects the weighted IL.

5.3.4 No Wagon: A - Weighted Total

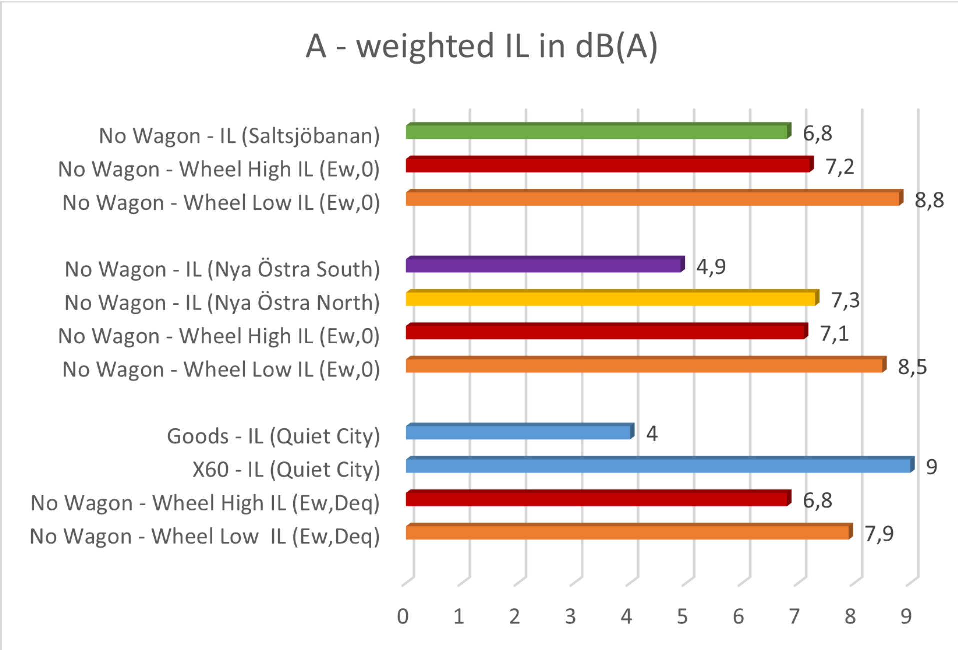

Figure 5.21: A - weighted IL of the different "No wagon"-model receivers in comparison to their respective reference measurements.

6
Discussion

In this chapter the results will be analysed. Furthermore the various difficulties encountered and suggestions for possible future improvements are discussed.

6.1 The Results

A reoccurring pattern that can be noted in most of the results are the fluctuations of the 1/3-octave band results in relation to the measured data from the literature used as reference . This is suspected to be because of an inaccurate impedance-model used for the ballast and the inner side of the screen. As a significant part in the function of a LHNS is to basically trap the sound beneath the train car and attenuate it though multiple reflections, the inability to apply the correct impedance to the surfaces will be a cause of errors. This is especially true in the case of BEM. In hindsight this should have been a major focus and is perhaps even more important than the ability to use more complex geometries.

The results in Figure 5.2 showed a fairly good fit to the reference data. However at 800 Hz there is a clear divergence. As mentioned in section 2.4.1 there is an upward shift in source height for the energy distribution with increasing frequency. Based on this information alone a decrease in the insertion loss is to be expected in the higher end of the spectrum. However, because of the way the X60 train is constructed, the high wheel source is not possible without colliding with the train body.

If the case without a wagon is studied in Figure 5.16 there is no boogie, thus the high wheel source placement is possible and a considerable lowering of the insertion loss can be seen as the frequency get higher. But even when the boogie is removed and the source is weighted, the insertion losses are still considerably higher compared to the reference measurements. Furthermore, because of the way the X60 is modelled (and constructed) a large portion of the sound energy is expected to be attenuated in the volume beneath the boogie. Because of this a higher source placement in this area is not expected to achieve a lower insertion loss.

If Figure 5.1, 5.3 and 5.5 are compared to the corresponding cases without a wagon in Figure 5.15, 5.17 and 5.19 this is quite clear. When the body of the X60 wagon is included, the wheel source placement achieves an even larger insertion loss than that of the rail source, over almost the entire spectrum compared to up to about 315 Hz for the case with no wagon. By this reasoning the cause of the divergence is suspected to be because of something else, such as an inaccurate impedance model causing erroneous absorption: This, combined with resonances in the model that are not present in a real train, could cause significant differences in the attenuation. One other thought is that more sound than anticipated could be emanating from the boogie and because of the low speed, the relative contribution of, for example an air-conditioner fan, is significant.

One other variable that could cause problems are the acoustical near fields. However, in this thesis complex frequencies of up to 150 Hz were included in the calculations. This limit was decided to be well within reason because the smallest source-receiver distance is 7.5 m and the fact that near-field decay significantly with distance. Thus the near fields should not produce a significant error contribution unless the receiver is placed close enough to the train.

If the cases of the roughly estimated industrial wagon in Figure 5.8, 5.10 and 5.12 are compared to the corresponding cases without a wagon the significant influence any addition of geometry apart from the ballast and screen can achieve is quite clear. In these cases the large differences are most likely due to that the body is situated at a height above the LHNS and that the body has infinite impedance. As an effect, some of the sound will be directly reflected to the receivers thus lower insertion losses are expected in relation to the other cases.

Now, having analysed the results more closely. The pattern of divergence from the reference measurements, and other unexpected behaviour, show correlation to increasing frequency. Returning to the reasoning that the error could be caused by an incorrect impedance model in combination with resonances: At 800 Hz the wavelength is approximately 0.43 m and would fit into the volume beneath the train in all directions. Thus, there could be resonances in an area where the absorbing surfaces provide erroneous absorption. With this reasoning it can be said, with some degree of certainty, that the inaccurate impedance model is an explanation to why the result are varied, and should be regarded as a major contributing error source. That said if any continuation is made on this work, the impedance model is a highly recommended place to start. Also, the points discussed regarding the sources could be addressed by conducting case specific measurements.

If Figure 5.7, 5.14 and 5.21 are studied it is clear that the low height noise screen implementation produce a significant insertion loss. Two major outliers can however be noted, "Goods - $IL_{QuietCity}$" and "$IL_{Nya\text{Ö}straSouth}$". The lower insertion loss of the "Nya Östra South" case is suspected to be because of the increased distance the south going track has to the implemented low height noise screen. As of why the levels of the goods-train in the "Quiet City" measurements are significantly lower is most likely due to noisy wagons. A noisy wagon could cause a larger source energy distribution at heights above the effective height of the low height noise screen. Thus a lower insertion loss is expected. With this reasoning, for the "$IL_{Nya\text{Ö}straSouth}$" and "Goods - $IL_{QuietCity}$", the differences between the simulated measurements and the measurements used as reference caused far greater deviations than initially expected. Therefore they should be omitted when compared to the insertion loss of the other cases. The resulting levels show a maximum deviation of 2.2 dB(A) if two major outliers in the comparison are excluded. They are therefore considered to have a good agreement with the reference data when describing the total sound pressure from the train.

6.2 Difficulties and Uncertainties

The description of the difficulties encountered in this project could be condensed down into to two categories; source energy distribution and numerical implementation.

6.2.1 Source Energy Distribution

One thing that became apparent was the clear lack of information regarding the energy distribution between the different sub-sources of a train. Only one source of information on the subject was found and this source only focused on the X2000 model. These data alone are not enough to provide for sufficient certainty, especially because of the suspected influence of the very train-model specific cooling fans. If more information regarding this subject is found or further research is made, it would be most beneficial to revisit and make further considerations regarding the source models.

6.2.2 Numerical Implementation

One of the main attenuating factors of the LHNS is the absorption in the numerous reflections between the screen and the train. To properly account for this the model was revised and the ability to add several shapes with more complex geometries were introduced. This would allow the modelling of an as close to real-life scenario as possible. However, the increase in computational load caused by this addition was underestimated. This lead to the decision to reduce the calculated spectrum to 25 Hz-3150 Hz. To enable higher spatial- and frequency resolution and an increased frequency spectral range, further optimisation of the implementation is advised. Some success in reducing the computation time was made by introducing parallel processing and could possibly be explored further. One other recommendation is to use an optimised data-cluster to perform the final calculations, this was explored but in the end not available to this thesis.

One thing that affected the outcome was that about halfway through the project a major flaw was detected in the revised version of the code and the debugging of this consumed a considerable amount of time. This resulted in that some intended improvements, such as a rework of the impedance model was not completed. As of now the model is only capable of using one type of impedance. As discussed in the results, this will contribute to the error as the impedance of the ballast and screen will not be the same.

Another challenge regarding the impedance was the decision on what model to use. To account for the porosity of both the Vitrumite in the S-block and of the ballast, a model for porous material was needed. The choice in the end stood between the Slit-Pore and the Hamet impedance models. But no data on the ballast-parameters at the sites of the reference measurements was available. Instead a very lengthy and cumbersome process of investigating what parameters in a reasonable range based on research made in [27] and [28] could achieve the best fit to the reference data.

6.3 Recommended Future Improvements

A great deal of the uncertainties regarding the outcome of this thesis stem from the suspected errors introduced by the inaccurate impedance model. By enabling the ability to add different impedance models to the surfaces in the regions where absorption is most important, the accuracy of the results will most likely improve.

The results used as reference were not specifically intended for usage in a validation process of this model. Whereby a separate validation process using a designated test setup is advised. Such a test should focus on gathering a more complete set of data. This should include, but not be limited to:

- Measurements in accordance to SS-EN ISO3095:2013 on several passes of one train type
- Measurements on a model using loudspeakers to simulate the train sources
- Parameters of the ballast at the measurement site
- Other important parameters that affect the outcome such as nearby buildings etc.

7
Conclusion

The purpose of this thesis was to investigate what methods could be used to accurately estimate the insertion loss of a low height noise screen. A literature-study showed that the conventional methods from the commonly used propagation models could not achieve this without the addition of complementary numerical simulations. Furthermore the study showed that a method called the 2.5D-BEM had previously been successfully used to achieve this.

To achieve as accurate results as possible one of the major areas of focus became how to model a train as a source. This included how the geometrical design of specific train models and how the relative energy distribution of the sub-sources in those models would influence the insertion loss. To achieve this a readily available MATLAB-script was complemented with the ability to handle more complex geometries.

However, there was a lacking nuance in the research regarding the relative energy distribution. This made for uncertainties in the comparison between the simulations and the measurements used as a reference. Furthermore a proper way to implement the correct impedance to every possible surface has yet to be implemented. This is suspected to be one of the major error contributors and should therefore be developed further.

As the scope of the thesis did not allow for a designated validation process, measurements from other projects had to be used to validate the model. Because of source and receiver related uncertainties about these measurements, and that they do not provide detailed information about most of the parameters needed to properly tune the model to the measurement. A complementary trail-and-error process had to be used to achieve agreement between the model and the reference measurements.

Due to the uncertainties caused by the relative source energy contribution and the implementation of the impedance model, any definitive conclusion regarding the functionality of the model should not be made without further improvement and validation.

With this said, modifications made to the model now enable the ability to use more complex geometries any future work have a solid basis on which to build upon. The results show that a consistent and considerable insertion loss can be achieved by the implementation of a low height noise screens, and the 2.5D-BEM model. The model show great promise in providing the Swedish Transport Administration with a method on which to build a good basis in their future planning process. The results of this thesis definitely warrants further consideration of implementing low height noise screens as a noise reducing device for the transportation infrastructure in Sweden.

Bibliography

[1] ÅA, "Patentsök - zbloc norden," 2016. [Online]. Available: https://sbloc.se

[2] Naturvårdsverket and Banverket, "Nord96 - buller från spårbunden trafik nv 4935," Naturvårdsverket, Tech. Rep., 1998.

[3] X. Zhang, "Tuning of the acoustic source model aiming at accurate noise assessments along high-speed railways," SP, Tech. Rep., 2015.

[4] B. Södergren, "Fordonsprofiler, dimensionering av järnvägsfordons yttermått," Trafikverket, Tech. Rep., 2015.

[5] Z. Norden, "S-block 250 - catalogue," 2016. [Online]. Available: https://sbloc.se

[6] H. G. Jonasson and S. Storeheier, "Nord 2000. new nordic prediction method for rail traffic noise," SP, Tech. Rep., 2001.

[7] J. Nielsen, O. Lundberg, and N. Renard, "Rapport quietcity bro," Quiet City, Tech. Rep., 12 2008.

[8] V. Wetterblad, "Saltsjöbanan - saltö - järla - storängen," ÅF - Konsult, Tech. Rep. RAPPORT 589476-A, 2013. [Online]. Available: www.afconsult.com

[9] P. Ragnarsson, O. Markstedt, T. Ab, O. Hellström, F. Arkitekter, and J. Magee, "Skogås(nya östra skolan) rapport," Acoustic Control, Tech. Rep., 2005. [Online]. Available: www.acoustic.se

[10] P. D. Stoor and UHtsv, "Utredning av spårnära bullerskärmar," Trafikverket, Tech. Rep. TRV2018/95460.

[11] C. Burgos and L. Wåssén, "A combination of a road restraint sys-tem and a noise reducing device," Master's thesis, Chalmers University of Technology, 9 2017.

[12] "Infrastrukturprofiler," Trafikverket, Tech. Rep. TRVINFRA-00004, 2021.

[13] "Bullerskyddsskärm järnväg," Trafikverket, Tech. Rep. TRVINFRA-00010, 2021.

[14] G. Grundfelt, "Tyréns - akustiskt prestanda z-bloc," Tyréns, Tech. Rep., 2015. [Online]. Available: www.tyrens.se

[15] B. Plovsing and J. Kragh, "Nord2000. comprehensive outdoor sound propagation model. part 1: Propagation in an atmosphere without significant refraction," DELTA, Tech. Rep., 2001. [Online]. Available: www.delta.dk

[16] P. Jean, M. Baulac, J. Defrance, and F. Minard, "Efficiency of noise protections in urban areas: Predictions and scale model measurements," *Acta Acustica-ACUSTICA*, vol. 92, pp. 530–539, 2001. [Online]. Available: https://www.researchgate.net/publication/233528821

[17] M. Baulac, J. Defrance, and P. Jean, "Optimization of low height noise protections in urban areas," Forum Acusticum, Tech. Rep., 2005.

[18] P. Jean, J. Defrance, and Y. Gabillet, "The importance of source type on the assessment of noise barriers," *Journal of Sound and Vibration*, vol. 226, pp. 201–216, 9 1999.

[19] D. Duhamel, "Efficient calculation of the three-dimensional sound pressure field around a noise barrier," *Journal of Sound and Vibration*, vol. 197, pp. 547–571, 11 1996.

[20] P. Jean, "A variational approach for the study of outdoor sound propagation and application to railway noise," *Journal of Sound and Vibration*, vol. 212, pp. 275–294, 4 1998.

[21] A. Jolibois, "A study on the acoustic performance of tramway low height noise barriers: gradient-based numerical optimization and experimental approaches," Ph.D. dissertation, EST Paris, 2013. [Online]. Available: https://www.researchgate.net/publication/260045179

[22] B. van der Aa and V. Group, "Road traffic noise reduction by multiple scattering and absorption mechanisms," Ph.D. dissertation, Chalmers University of Technology, 2015.

[23] J. Forssén, "Auralizing position-dependent abatements for a moving, extended source using a reference-case recording," Chalmers University of Technology, Tech. Rep., 8 2019.

[24] X. Zhang, "Prediction of high-speed train noise on swedish tracks," SP, Tech. Rep., 2010.

[25] "Rail transport in sweden - wikiwand," last accessed 2022-05-24. [Online]. Available: https://www.wikiwand.com/en/Rail_transport_in_Sweden

[26] "Morgondagens depåer, delrapport 4 sida 1 av 23," Transrail AB, Tech. Rep. [Online]. Available: https://fudinfo.trafikverket.se/fudinfoexternwebb/Publikationer/Publikationer_002501_002600/Publikation_002568/

[27] K. Attenborough, P. Boulanger, Q. Qin, and R. Jones, "Predicted influence of ballast and porous concrete on rail noise," Tech. Rep., 2017. [Online]. Available: https://www.researchgate.net/publication/289023361

[28] K. Attenborough, "Outdoor ground impedance models," in *Outdoor ground impedance models*. DC/ConfOrg, 2015, pp. 1785–1790.

[29] M. Mitchell, "Engauge digitizer," 2016. [Online]. Available: http://markummitchell.github.io/engauge-digitizer/

[30] J. Forsén and F.-X. Bécot, "4 integral equations for the sound field including boundaries." [Online]. Available: http://www.ta.chalmers.se/education/course-materials/

A

Appendix A

The surfaces of both the train(S_T), the ballast and the screen(S_{BS}) are enclosing the volumes V_T and V_{BS} respectively. Then if g and p are two continuously differentiable functions describing the behaviour at some point on the surfaces they can be formulated as

$$\int_V g\Delta p - p\Delta g dV = \int_S g\frac{\partial p}{\partial n} - p\frac{\partial g}{\partial n} dS \tag{A.1}$$

where Δ is the Laplace operator,$\frac{\partial}{\partial n}$ is the directional derivative outward from either surface S_T or S_{BS}. If p then is chosen to satisfy the Helmholtz equation

$$\Delta p(x) = q(x)k^2 p(x) \tag{A.2}$$

where q is some source function, k is the wave number and g is some variant of Green´s function[1] fulfilling

$$\Delta g(x|x_0) = \delta(x - x_0) - k^2(x|x_0) \tag{A.3}$$

where δ is the delta function. The left hand side of equation A.1 can then be written as

$$\int_V (g\Delta p - p\Delta g)\ dV = \int_V (gq - k^2 gp - p\delta + k^2 pg)\ dV = \int_V (gq - p\delta)\ dV \tag{A.4}$$

The integral over the delta function can be computed as

$$\int_V p(x)\delta\left(x - x_0\right) dV = p\left(x_0\right) \cdot \begin{cases} 1, & x_0 \text{ inside } V \\ \frac{1}{2}, & x_0 \text{ on } S \\ 0, & x_0 \text{ outside } V \end{cases} \tag{A.5}$$

Factors 1 and 0 can be found if the definition of the delta function is studied and the factor 1/2 can be derived from the limit of equation A.1 when the receiver approaches S_T or S_{BS}[30]. By assuming that the enclosing surfaces have a normalised impedance of

$$\beta = \frac{\rho c v_n}{p} \tag{A.6}$$

and utilising Euler´s equation

$$\frac{\partial p}{\partial n} = -j\omega\rho v_n = -jk\beta p \tag{A.7}$$

[1]Could be for free-space, changing sound speeds or reflections from surfaces with impedances etc.

equation A.5 can be written as

$$\left.\begin{matrix} 1 \\ \frac{1}{2} \\ 0 \end{matrix}\right\} \cdot p\left(x_0\right) = \underbrace{\int_V g \cdot q \; dV}_{p_0(x_0)} + \int_S g \cdot jk\beta p \; dS - \int_S p \frac{\partial g}{\partial n} \; dS \tag{A.8}$$

where p is some unknown pressure amplitude along the surface S. If g is assumed to be Green´s free space function

$$g = \frac{1}{4\pi R} e^{-jkR} \tag{A.9}$$

then its directional derivative is

$$\frac{\partial}{\partial n} g = -\frac{1}{4\pi R}(jk + \frac{1}{R}) e^{-jkR} (\vec{e}_R \bullet \vec{n}_S) \tag{A.10}$$

equation A.8 can be written on the form of a Kirchhoff-Helmholtz Integral equation

$$\begin{aligned} \left.\begin{matrix} 1 \\ \frac{1}{2} \\ 0 \end{matrix}\right\} \cdot p\left(x_0\right) = \frac{1}{4\pi} \int_V \frac{e^{-jkR}}{R} \cdot q \; dV + \frac{1}{4\pi} \int_S \frac{e^{-jkR}}{R} \cdot j\omega\rho v_n \; dS ... \\ -\frac{1}{4\pi} \int_S p \frac{e^{-jkR}}{R} \left(jk + \frac{1}{R}\right) (\vec{e}_R \bullet \vec{n}_S) \; dS \end{aligned} \tag{A.11}$$

B
Appendix B

To get a good idea of the error margins and the accuracy of the implemented code a series of test-simulations was conducted.

To not cause problems caused by an excessive amount of chief points in relation to the amount discretised elements on the surfaces the amount is set as a function of frequency and a specific number of points per wavelength fitting in some maximum distance. The tuning process can be seen in Figure B.1 where CHIEFPPW is the amount of chief points per wavelength fitting. Convergence was troublesome to find below the 63 Hz band. The reason the unexpected behaviour of the CHIEFPPPW6 data was investigated and is still unknown. It is therefore considered as an outlier. If a value of more than 5 points are used there is a clear convergence. In the end a value of 5 points per wavelengths is used as it offers a good trade off between accuracy and computational load.

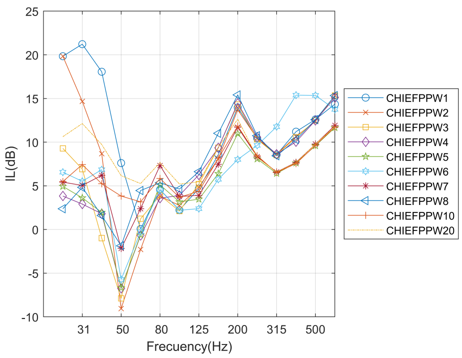

Figure B.1: Test of an increasing amount of chief points per wavelength fitting in the structure.

In Figure B.2 the tuning process of the spatial resolution is presented. The resolution should be high enough to give good accuracy, but also low enough to not increase the computational load to much. Here a clear convergence can be seen above 125 Hz. The value of 6 points per wavelength is used in the simulations in this thesis.

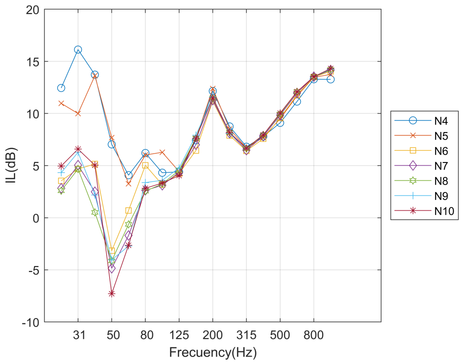

Figure B.2: Test on an increasing amount of discretised points per wavelength C_{ppw}.

DEPARTMENT OF ARCHITECTURE AND CIVIL ENGINEERING
CHALMERS UNIVERSITY OF TECHNOLOGY
Gothenburg, Sweden
www.chalmers.se